PART I

METHODOLOGY

CHAPTER 1

Introduction to Mass Spectrometry

SCOTT A. SMITH

Department of Chemistry, Michigan State University, East Lansing, MI 48824

RUTH WADDELL SMITH

Forensic Science Program, School of Criminal Justice, Michigan State University, East Lansing, MI 48824

YU XIA

Department of Chemistry, Purdue University, West Lafayette, IN 47907

ZHENG OUYANG

Weldon School of Biomedical Engineering, Purdue University, West Lafayette, IN 47907

1.1 HISTORY

Although mass spectrometry (MS) has aged by about one century, it has never ceased to evolve into an increasingly powerful and important technique for chemical analysis. The development of mass spectrometry can be folded into a few periods, where the capabilities of a particular discipline of science were advanced significantly and steadily due to the introduction of MS into that field. Those periods are, approximately, physics (1890s–1945), chemistry (1945–1975), materials science (1955–1990), and biology/medicine (1990–present) [1]. The history of MS shows that the technique has facilitated many significant scientific achievements, from the discovery of isotopes [2], to purifying the material for the first atomic bombs [3], to space exploration [4,5], to the mass analysis of whole red blood cells each weighing several tens of picograms [6]. The following is a short account of some of the notable feats that have transpired in this field.

Characterization of Impurities and Degradants Using Mass Spectrometry, First Edition.
Edited by Birendra N. Pramanik, Mike S. Lee, and Guodong Chen.

1.1.1 Atomic Physics

The technique now known as MS has its roots in atomic physics at the beginning of the twentieth century, when it was originally applied by physicists toward answering questions on the nature of atoms. Throughout much of the 1800s, the prevailing wisdom held that atoms were indivisible, that all atoms of a given element had the same mass, and that the masses of all elements were multiples of the mass of hydrogen [7–9]. Despite these beliefs, the interrogation of bulk elements through chemical means (gravimetric analyses) demonstrated that some atomic masses were, in fact, not unit integers of that of hydrogen (e.g., chlorine). Furthermore, for much of the century, relatively little was known of the nature and origins of electricity. Hence, the explanations for these phenomena awaited the discovery of electrons and isotopes through physical investigations.

Toward the end of the 1800s, many physicists were interested in unraveling the underlying principles of electricity. To study the properties of electric currents, they would create a potential difference between two electrodes in partially evacuated discharge tubes made of glass and containing various types of gas. Evidence for *cathode rays* (electron beams) was first observed by Plücker in 1859 when he noticed a green phosphorescence occurring on his discharge chamber at a position adjacent to the cathode [10]. In time, the investigations of other physicists led to an accumulation of clues about the nature of cathode rays, including observations that (1) they are directional, moving from the cathode to the anode, (2) they are energetic, as determined by observing platinum foil becoming white-hot when placed in their path, (3) they conduct negative charge, as determined by measurement with electrometers, (4) they are particles rather than waves, (5) their energy is proportional to the acceleration potential to which they are subjected, (6) they have dimensions that are smaller than those of atomic gases, as determined by considering their penetration depth through media of varying density, and (7) they may be derived from any atom through various means, including heat, X rays, or electrical discharge [10]. Thomson went on to develop the means for measuring electron mass in a discharge chamber evacuated to low pressure (see Figure 1.1) [11]. By applying a magnetic field (B) and an electric field (E), both at right angles to each other as well as to the direction of electron propagation, they could determine the electron velocity (v) by canceling out the deflections of the magnetic and electric forces (i.e., $|Bev - Ee| = 0$) such that the electrons travel in a straight line, yielding $v = E/B$. The ratio of electron mass to electron charge (m_e/z) could also be arrived at from experimental measurements as $(m_e/e) = (B^2 l/E\theta)$, where l is the distance traveled by an electron through a uniform electric field and θ is the angle through which electrons are deflected as they exit the electric field [11]. From this and other experiments, Thomson demonstrated that the mass of electrons are about $\frac{1}{1000}$th(0.001%) that of the proton (the mass of protons, the ionized form of the smallest known particles at the time, was by then known from electrolysis research) [11]. Thomson was awarded the 1906 Nobel Prize in Physics "in recognition of his theoretical and experimental investigations on the conduction of electricity by gases" [12].

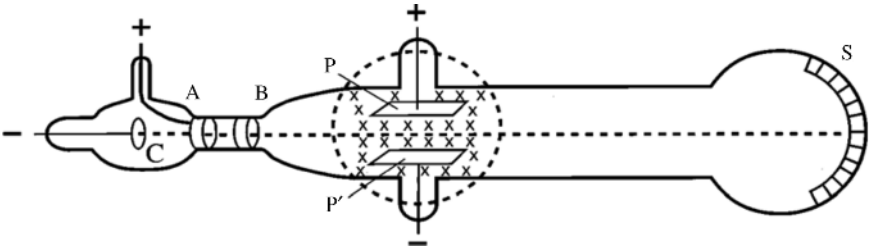

FIGURE 1.1 Thomson's apparatus for measuring electron mass-to-charge ratio (m/z). Components are as follows: (A, B) anodes with pinhole apertures to guide and narrow the beam; (C) cathode; (P, P′) electric field deflection electrodes; (S) detection screen. The magnetic field, when applied, was directed orthogonally to both the electron beam and the electric field (indicated by the tickmarks x). (Reprinted from Ref. 10, with permission of John Wiley & Sons, Inc.)

While progressing toward an understanding of electrons, physicists also became interested in understanding the positively charged particles (cations) that were present in discharges [13]. During studies of the effects of weak magnetic fields on cathode rays in 1886, Goldstein discovered positively charged *anode rays* that traveled in the opposite direction of electrons; unlike cathode rays, these anode rays were not susceptible to deflection by the weak magnetic fields used in Goldstein's experiments [14]. However, in 1898, Wein determined that anode rays in fact could be influenced by the presence of magnetic fields, provided the fields were relatively strong; with this knowledge, he determined that their masses were on the order of atoms rather than the substance of which cathode rays were composed [14]. Building on such early observations, Thomson created a device called the *parabolic mass spectrograph* (see Figure 1.2), in which he exposed anode rays to parallel magnetic and electric fields in such a way that, while propagating through the field region the rays were influenced vertically by the electric field and horizontally by the magnetic field, with the result that the ions impinged on a photographic plate positioned transverse to the direction of particle propagation [14]. The images on the plate were of parabolas, in which each particular parabola was specific for mass-to-charge ratio (m/z) and the occurrence of parabolic lines was attributed to distributions in kinetic energy [14]. Thomson's device was capable of identifying the presence of ionized gases, and he demonstrated its capabilities by acquiring a mass spectrograph of the mixture of gases constituting the atmosphere [14]. Notably, Thomson's atmospheric data showed the first instance of the rare isotope ^{22}Ne (neon-22) adjacent to the predominant ^{20}Ne; since he believed that stable elements could have only a single mass (a then widely held belief), he assumed that what was conventionally considered neon was actually a mixture of two elements, with that at mass 22 being previously unknown [2,14]. Shortly before this time, Rutherford and Soddy discovered nuclear transmutation, whereby fission products from radioactive elements produce as products chemically distinguishable elements of abnormal mass (i.e., *isotopes*) [15]; however, given the unusual nature of radioactive matter at the time of Thomson's observation, the link was not obvious that neon atoms could occur as distributions

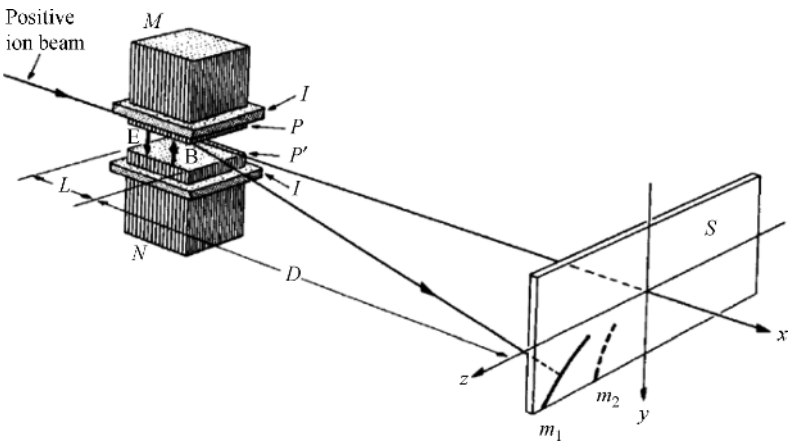

FIGURE 1.2 Ion separations on Thomson's parabolic mass spectrograph. Components are as follows: (I) insulator; (M, N) magnet poles; (P, P′) electric field deflection electrodes; (S) detection screen. The position of ion impact (shown here for two species labeled m_1 and m_2) on the screen was dependent on ion charge and kinetic energy, the electric and magnetic field strengths, and the dimensions of L and D. (Reprinted from Ref. 10, with permission of John Wiley & Sons, Inc.)

of varying mass. It wasn't until 1919, when Aston built an improved mass spectrograph and discovered the isotopes of dozens of elements, that isotope theory became widely accepted by the scientific community [16]. When he published the results of the measurements of the first 18 elements that he investigated, Aston demonstrated that they all were within $\frac{1}{1000}$th of whole-number units, with the exception of hydrogen, which has a very slight deviation from the whole-number trend [16]. For his efforts toward proving the existence of isotopes, Aston won the 1922 Nobel Prize in Chemistry.

The first breakthroughs in MS were made using equipment that required manual measurements of mass based on visual observation or the interpretation of photographic records that were prone to indicating disproportionate signal intensities based on the species analyzed [13]. These issues were resolved with the development of the first mass spectrometer, by Thomson, in 1912 [13,17]. Rather than detecting on an *image plane* under conditions of constant field strength (as in the mass spectrograph), in Thomson's mass spectrometer the field strengths to which the ions were exposed could be systematically varied while the ion intensities were acquired as electric current using an electrometer positioned behind a plate containing a parabolic slit [13]. This modification also removed a mass dependence on detection intensity, as a signal intensity bias existed on the photographic plates of the spectrograph that favored ions of lower mass, a feature that would be critically detrimental to accurate measurements of relative abundance [13].

As time passed, other physicists made improved mass spectrometers. In 1918, Dempster built a mass spectrometer featuring electronic detection and a 180° magnet capable of resolution values of around 100 (for atomic-range masses) [17]. Aston

constructed several notable mass spectrometers; his first, in 1919, was a tandem-in-space *EB* configuration that featured energy correction (i.e., ions of a given *m*/*z* arrived at a single point on the detection plane regardless of the velocity distribution within the beam) that was capable of achieving a resolution of $\leq$130; later versions of a similar design achieved resolutions of 600 (in 1927) and 2000 (in 1942) [18]. In 1939, Nier produced a magnetic sector instrument that was much smaller than Dempster's (i.e., a few hundred pounds vs. 2000 lb) that was the basis for the design of all future magnetic sectors [19]. With isotope-based research taking off, various other teams also took up the challenge of creating better instruments and developing new applications.

1.1.2 Early Applications

Early applications of MS were centered on discovering isotopes and measuring their relative abundances. By 1935, all known elements in the periodic table had been evaluated for their isotopic compositions by MS [13]. As mass accuracy and precision improved, MS eventually supplanted gravimetric analysis as the predominant method for measuring atomic weights [18]. Another use for MS in the 1930s was for the dating of minerals (*geochronology*) by measuring the relative abundances of radioisotopes in a given sample; for example, by considering a sample's radioisotope ratios in the context of known rates of radioactive decay, the current age of Earth has been determined to be about 4.5 billion years [13]. Mass spectrometers may also lend themselves to separating radioisotopes in a preparative fashion, as in the case of uranium; an early attempt at such processing resulted in the separation and retrieval of some nanograms of the rare ^{235}U from the predominant ^{238}U—an amount sufficient to demonstrate for the first time that ^{235}U is the uranium isotope that readily undergoes fission reactions [19]. Interest in the use of fissile material in weapons ensued, and by spring 1945 hundreds of massive sector instruments ("calutrons") were operating in Oak Ridge, Tennessee to produce some of the ^{235}U used against the people of Hiroshima, Japan in World War II [3]. Although fairly quickly supplanted by the more efficient gas diffusion methods of ^{235}U purification, mass spectrometers nonetheless remained invaluable for enriched materials production for their use as leak detectors and for purity confirmation of the gas diffusion process [19]. It was also during this period that MS was applied toward another very different application—as a means of characterizing the molecular structure of hydrocarbons during crude oil processing [13].

1.1.3 Organic Structural Analysis

Driven by analytical demands from the petroleum and pharmaceutical industries for the characterization of refined petrochemicals and natural products, respectively, MS began to transition into its role as a powerful tool for molecular analysis. The early challenges of such applications were many, including sample introduction, hardware reliability, and spectral interpretation; the latter was particularly difficult as the fundamental rules of structural analysis took years to develop. The invention of

electron ionization by Dempster in 1929 went a long way toward ensuring analytical reproducibility among different instruments, the basis for a community-wide effort toward developing a systematic approach for molecular structure interpretation. Rules were established to explain characteristic fragmentation patterns in mass spectra; an example was the "nitrogen rule," which could be applied to organics to interpret which peaks might contain nitrogen or alternatively to determine whether particular peaks corresponded to even- or odd-electron ions if the analyte is of a known composition. Mechanisms were derived to explain dissociation processes; well-known examples include those of metastable ions (where ion internal energy is sufficient for dissociation of an ionic system, yet the system does not fully fragment prior to detection, resulting in a broadened peak) [20] and the McLafferty rearrangement (intramolecular proton abstraction to a carbonyl oxygen from a γ-hydrogen) [21]. The structural analysis of hydrocarbons and other small organics was systematically delineated in McLafferty's seminal text *Interpretation of Mass Spectra* (ca. 1966 but updated as recently as 1993) [22,23]. As chemists became more confident in their spectral interpretation capabilities, the experiments they tried also increased in complexity; to meet these challenges, instrumentation became more sophisticated. Innovations such as tandem MS (MS/MS) [24] for stepwise fragmentation analysis and the coupling of gas chromatography with MS (GC-MS) [25] did much to improve the information attainable by MS as well as its applicability toward the analysis of complex mixtures. Insights into thermochemistry also began to be derived from MS. Ionization potentials for molecular ions and appearance energies for product ions could be determined through various methods, allowing the determination of chemical properties of isolated ionic systems [26].

1.1.4 The Biological Mass Spectrometry Revolution

By the early 1970s, MS was a mainstay in many analytical laboratories. In fact, the technique was also deemed essential outside the laboratory and off the planet as well, having been sent on the *Viking* space mission to Mars in 1976 [27]. Through the decade, commercialized versions became available for various platforms, including sectors, GC-MS (featuring quadrupole filters), time-of-flight (TOF), and Fourier transform ion cyclotron resonance (FT-ICR). The analysis of small organics had become relatively routine, and a major emphasis of research turned toward the problems of biology and the analysis of large, fragile biomolecules such as peptides and proteins. Although Biemann and coworkers had shown the potential for mass spectral sequencing of small peptides in 1959 [28], much was still to be done to improve the effectiveness of bioanalysis. Techniques that showed early promise in biomolecule analysis included desorption methods such as fast-atom bombardment (FAB) and liquid secondary ionization MS (LSIMS), where bombardment of a liquid sample matrix with high-energy neutral or charged particles (respectively) can facilitate the ejection of intact pseudomolecular ions; another technique applied to early protein analysis was plasma desorption MS (PDMS) [29], where bombardment of a surface-deposited sample by ^{252}Cf fission fragments could result in the expulsion of large ionized molecules that were predeposited on the surface. However, the

glycerol matrix of FAB/LSIMS techniques can lead to high background, and the equipment for PD was limited to only a small number of laboratories. The advent of thermospray, the ionization of LC eluant in a heated vacuum interface, proved promising in that it allowed the online coupling of liquid chromatography to MS (i.e., LC-MS) for the analysis of nonvolatiles; however, thermospray is seldom employed today as its performance was surpassed by electrospray, a somewhat similar technique that was developed in the mid- to late 1980s by Fenn [30]. Fenn approached the issue of protein analysis by using a technique known as *electrospray ionization* (ESI) [31], whereby large biomolecular ions could be formed via the nebulization of an electrified liquid. Much headway was being made in the area of laser desorption in the 1980s, culminating with the mass analysis of very large intact biomolecular ions: Tanaka developed a method using UV-resonant metal nanoparticles to enable the intact ionization and volatilization of proteins, while Karas and Hillenkamp developed a similar technique which they termed, *matrix-assisted laser desorption ionization* (MALDI), wherein preformed ions reside in a solid matrix prior to their ejection by the UV photoexcitation and explosion of organic matrix crystals [32,33]. For their efforts toward establishing protein analysis by MS, Tanaka and Fenn shared the 2002 Nobel Prize in Chemistry.

Since the relatively recent establishment of proteomics (the study of protein structure and function) [34], other "omics" studies have also been developed using similar strategies, including metabolomics, lipidomics, glycomics, metallomics, and phosphoproteomics. Remarkable biological insights have resulted, including the protein sequencing of fossilized dinosaur remains [35]. Relatively recent contributions to instrumentation have included the successful introduction of a new ultra-high-resolution mass analyzer (the Orbitrap™, originally developed by Makarov at Thermo Fisher Scientific, Bremen, Germany) that can match the high-performance capabilities of FTICR for a fraction of the cost. The chemical imaging of tissues using MS shows promise for a future of highly enhanced medical and biological investigations [36]. New methods of ion activation have also been developed and applied toward biological problems, including electron capture dissociation (ECD) [37] and electron transfer dissociation (ETD) [38]; these two similar techniques are notable for their radical-directed dissociation mechanisms, which allow the analysis of proteins carrying posttranslational modifications (PTMs), whose locations would otherwise often be unidentified in analyses using conventional methods of activation [i.e., collision-induced dissociation (CID)]. The future of MS promises to resolve many more biological issues with ever-greater performance.

1.2 IONIZATION METHODS

Chemical analysis using MS is achieved by measuring the mass-to-charge ratios (m/z) of the charged forms of the analyte molecules. The first step in the mass analysis process is to generate the analyte as ionic species in the gas phase. A wide variety of ionization methods have been developed over the last several decades, which enabled

the utilization of MS in different areas of chemical analysis. The main challenge in the development has always been preserving the molecular information while converting the analyte molecules from condensed phases into gas phase and making them charged. Soft ionization methods allow the preservation of the molecular structures in ions, which can be elucidated with the combination of the MS and MS/MS analysis. The energy deposition required for transferring analyte molecules into the gas phase and ionizing them can easily result in intense fragmentation of the molecules, as in certain desorption ionization methods, inductively coupled plasma (ICP), and electron impact (EI) ionization. This problem becomes much more severe when applying MS for the study of biompolymers such as peptides and proteins, whose volatility is low but whose structural information is highly valuable. Development of the electrospray ionization (ESI) and matrix assisted laser desorption/ionization (MALDI) provided the solution for this problem. Since the ionization methods have been comprehensively described in the literature, including the recent volume of *The Encyclopedia of Mass Spectrometry* (Vol. 6, *Ionization Methods*) [39], we have listed the characteristic features of the most commonly used ionization methods in Table 1.1. Their implementation with different types of instrumental setups for several applications is discussed later in this chapter.

1.3 MASS SPECTROMETER TYPES

Mass spectrometry is a discipline of analytical chemistry wherein the gas-phase ionic form of chemical species may be identified and characterized according to their mass and the number of elementary charges that they carry. There are several divisions of instrumental aspects of mass spectrometers including sample introduction, ion formation, ion transport, mass analysis, detection, vacuum systems, and software. In the following text we will introduce the reader to the principles of the various mass analyzers, providing a brief but comprehensive overview of the practical aspects of operation. This introduction is not meant to be exhaustive; lesser-used techniques or unlikely phenomena are mentioned only in passing or not at all. In the following sections we briefly describe the principal mass analyzers used in MS: magnetic sector (B), quadrupole mass filter (QMF), quadrupole ion trap (QIT), time-of-flight (TOF) analyzers, Fourier transform ion cyclotron resonance (FT-ICR), and Orbitrap.

1.3.1 Magnetic Sector Mass Spectrometers

The separation of ions in a strong electric or/and magnetic field constitutes the oldest form of mass spectrometric analysis, with roots dating back to the end of the nineteenth century. Under the influence of strong direct-current (DC) electric (E) and magnetic (B) fields, a gas-phase ion population may be made to undergo separations within an E field based on ion kinetic energy ($0.5\,mv^2$) or within a B field based on momentum (mv). Some founding innovators in the development of magnetic analyzers (and indeed MS) included Wein, Thomson, Aston, and Dempster.

TABLE 1.1 Characteristic Features of the Most Commonly Used Ionization Methods

Ionization	Pressure	Suitable Analytes	Ionic Species	*m/z* Range
Inductively coupled plasma (ICP)	> mTorr	All	Atomic ion, A^+	< 220
Electron impact (EI)	< mTorr	Volatile organic compounds (VOCs)	Molecular and fragment ions, $M^{+\cdot}$, $M^{-\cdot}$	< 1000
Chemical ionization (CI)	~ 1 Torr	VOCs	Molecular ions $(M + H)^+$, $(M - H)^{-\cdot}$ $M^{-\cdot}$, and adduct formation	< 1000
Atmospheric-pressure CI (APCI)	Atmospheric	VOCs, metabolites	Molecular ions $(M + H)^+$, $(M + H)^+$, $(M - H)^{-\cdot}$ $M^{-\cdot}$	< 1000
Electrospray ionization (ESI)	Atmospheric	Metabolites, lipids, peptides, proteins	Multiply protonated/deprotonated molecular ions $(M + nH)^{n+}$, $(M - nH)^{n-}$, and complexes	< 4000
Matrix-assisted laser desorption ionization (MALDI)	< 1 Torr	Metabolites, lipids, peptides, proteins	Singly protonated/deprotonated molecular ions $(M + H)^+$, $(M - H)^{-\cdot}$ and complexes	≤200,000

Early applications of sector mass analysis included investigations of fundamental atomic physics: for example, the existence of and the mass of electrons [11], in addition to the accurate determinations of the masses and natural abundances of isotopes [2,16]. Sector analyzers have also been used for the isotopic purification of ^{235}U for the first atomic bomb [3], as platforms for the study of much of the earliest tandem MS experiments [20,40], and for accurate determination of the age of materials based on isotope ratios (e.g., carbon dating) [17]. As understanding of ion trajectories and their impact on mass spectrometric performance matured, instruments evolved with increasing sophistication; in time, sector instruments achieved such sophistication as to allow achievable resolutions of up to 10^5 and single-digit part-per-million (ppm) mass accuracies. Today, sector analyzers have largely been supplanted by other mass spectrometer types, although they are still employed for some applications (e.g., ultra-accurate isotope ratio determinations) [18]. With the rate of development of sector instrumentation and applications in decline for some time, recent literature discussions on the matter are principally available in MS texts [41–43].

When an ion is exposed to a magnetic field occurring in a dimension perpendicular to the ion's trajectory, the ion experiences a force in a direction orthogonal to both B and the ion's velocity. The circular path that an ion takes through a homogenous magnetic field is dependent on a balance between centripetal and centrifugal forces, which can be described as

$$zevB = \frac{mv^2}{r} \tag{1.1}$$

where z is the number of elementary charges on an ion, e is the elementary charge (1.602×10^{-19} C), B is the magnetic field magnitude, m is the ion mass, v is the ion velocity, and r is the radius of the ion trajectory as it is deflected by the magnetic field. Often, B sector analyzers are referred to as "*momentum analyzers*", as can be seen by rearrangement of Eq. (1.1) to arrive at

$$r = \frac{mv}{zeB} \tag{1.2}$$

Hence, for ions of a given charge and a constant magnetic field strength, the degree of deflection that an ion incurs as it transits through a magnetic sector is dependent only on momentum (mv).

A magnetic sector mass spectrometer can consist simply of an ion source, an electromagnet, various slits to allow selective ion beam passage prior to and after the mass analyzer, a vacuum system, an electrometer, and a data processor. Ions are generated in a source and then accelerated (by way of an electric field) toward the entrance of the B sector analyzer, where they experience a deflection dependent on their mass, charge, and velocity. For sector MS, the extraction potential at the source is quite high (e.g., 10 keV) to maximize sensitivity by reducing beam broadening, and also to allow for ions to pass quickly through a sector as it is being scanned without significantly affecting resolution. Since ion sources do not produce

monoenergetic ion beams, it is quite common to couple a magnetic sector mass analyzer in tandem with an electric sector analyzer such that the E sector can be made to select a range of ions having the same kinetic energy (E sectors are technically *energy analyzers* rather than mass analyzers). In such "double-focusing" geometries, correction is effected for both kinetic energy and angular dispersion in the electric and magnetic sectors, respectively. Kinetic energy correction is achieved in an E sector through a balance between centripetal and centrifugal forces, which is shown in the following equality:

$$zeV_{\text{accel}} = \frac{mv^2}{r} \tag{1.3}$$

which may be rearranged to consider ion trajectories along a circular arc:

$$r = \frac{mv^2}{zeV_{\text{accel}}} \tag{1.4}$$

Provided an ion beam is made monoenergetic by an E sector prior to mass analysis (as in the EB tandem configurations; e.g., see Figure 1.3), the m/z of the ions within the population may be determined by detection of ions either along an image plane or at a single point. For the former case, B is maintained at a constant value such that variation in ion m/z corresponds to variation in r, which results in ions arriving at different points along an image plane in an m/z-related manner (the image plane consists of either a photographic plate for early instruments or multicollector detectors for more modern ones). Such simultaneous broad-spectrum detection provides the highest sample efficiency, although achieving high resolution or sensitivity through such means requires stringent fabrication specifications for the detector [44]. Alternatively, given the means for scanning B, a tandem sector mass spectrometer may be operated in such a way that ions may be detected at a single position along the detection plane (e.g., at an electron multiplier behind a narrow slit). Such fixed-point detection is typically limited to a scan rate of 100 ms per decade

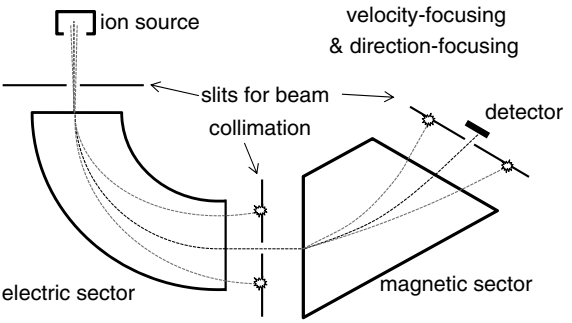

FIGURE 1.3 Depiction of an EB dual sector mass spectrometer. Ions are detected as a function of their deflections in the electric and magnetic sectors.

(e.g., from 100 to 1000 m/z), as higher scan rates can degrade resolution [42,43]. Additionally, the fact that B is scanned quadratically to achieve a linear correlation with m/z, and hence that m/z-dependent sensitivity and inaccurate relative abundances can occur, must be considered.

1.3.2 Quadrupole Mass Filter and Quadrupole Ion Trap Mass Spectrometers

Quadrupole mass analyzers separate ions through controlled ion motion in a dynamic quadrupolar electric field. First introduced by Paul and Steinwedel in 1953 [45], quadrupole mass analysis is performed on two types of mass analyzer: quadrupole mass filters (QMFs) and quadrupole ion traps (QITs). Common analytical traits of quadrupole mass spectrometers include "unit" resolution (i.e., differentiation of singly charged isotopes), mass-to-charge ratio (m/z) ranges of >1000 Th (Thomson; unit measuring m/z), and specific chemical structural information provided through tandem MS. The fundamental basis for ion stability is essentially the same for both analyzer types, yet some differences exist in geometry and the waveforms applied in order to produce mass spectra. The following information is intended only to convey the major principles of operation and their consequences on performance. For further and deeper discussions of the concepts associated with quadrupole MS, the interested reader is encouraged to explore several detailed reviews [46,47].

An *electric field* occurs when there is a potential difference between two objects. It is the nature of an electric field to store electrical potential energy, and ions in such a field may occupy any Cartesian coordinate position provided their kinetic energies match or surpass the electric potential energy (pseudopotential) associated with that position. A *quadrupole field* provides a linear restoring force as a function of the square of an ion's displacement from the field center. Hence, the form of the force F on an ion moving away from the trap center in a trapping dimension of a QIT is in accordance with Hooke's law for harmonic oscillation [48]

$$F(u) = -C \cdot u \tag{1.5}$$

for u is displacement in a dimension of ion motion and C is a constant. Given that ions enter a quadrupole mass analyzer with nonzero kinetic energy, they will undergo sinusoidal oscillation within the pseudopotential well of the radiofrequency (RF) field. The magnitude of ion displacement depends on the relative magnitudes of the ion and field energies, and ion position is restricted to those regions of the field with potentials that the ions can match or surpass given their own kinetic energy. The position and trajectory of an ion depends on its charge, mass, velocity, and starting position, and the repulsive or attractive forces of the electric field and other ions. Either the kinetic or internal energy of an ion may be modified through collisions between the ion and background gas or through Coulombic interactions between like- or oppositely charged ions. Given an understanding of ion behavior within an electrodynamic quadrupole field, an analyst can use a quadrupole mass spectrometer to manipulate and mass-selectively detect ions as mass spectra.

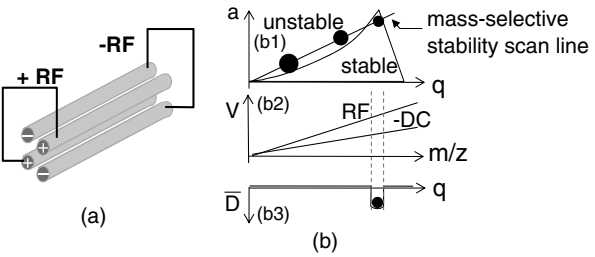

FIGURE 1.4 Depiction of some aspects of quadrupole mass filters: (a) isometric view of a quadrupole mass filter, where the electrodes are paired across the axis of the analyzer; (b) some principles involved in mass analysis — plot (b1) indicates relative positions of three ions in the *a*,*q* space of the Mathieu stability diagram; plot (b2) indicates the potentials applied as functions of ion seqular frequency; plot (b3) depicts the pseudopotential well depth, where the *m*/*z* of interest is shown in the only stable region.

In a QMF and, by analogy, QITs, an electric field occurs between two pairs of parallel electrodes, with each pair short-circuited together and situated opposite each other and equidistant about a central axis (see Figure 1.4). In ideal geometries, electrodes are of a hyperbolic form so as to provide the purest quadrupole electric potential (ϕ_2), which can be described mathematically for any point (x,y) in the cross-sectional plane of a QMF (for example) as [47]

$$\phi_2(x,y) = A_2 \frac{(x^2 - y^2)}{r_0^2} + C; \quad x^2 \leq r_0^2; \quad y^2 \leq r_0^2 \tag{1.6}$$

where x and y are displacements from the QMF center in their respective dimensions, r_0 is the inscribed radius of the QMF, A_2 is the amplitude of the applied potential, and C is a constant added to the potential to account for any "float" voltage applied equivalently to all electrodes, which is relevant for instances beyond the frame of reference of the quadrupole (e.g., the transport of ions into or out of the device). The lack of cross-terms between the Cartesian coordinates (e.g., xy) means that, in a quadrupole field, ion motion in each dimension is independent of the fields or motion in orthogonal directions; this feature makes it much easier to consider aspects of ion motion and manipulation in comparison to higher-order multipoles. The amplitude of the applied waveform A_2 is of the form

$$A_2 = \pm(U - V\cos(\Omega t)) \tag{1.7}$$

where U is the DC potential and V is the RF potential that oscillates at the angular frequency Ω and the plus/minus sign designates that the two rod pairs are of opposite sign. For QMFs, the force on an ion depends on its position within the electrodynamic field; at any given moment, an ion is simultaneously accelerated in two dimensions—attraction in one dimension and repulsion in an orthogonal dimension. For ions of stable trajectory, the potential on the electrode pairs will always reverse and attain sufficient amplitude to redirect ion trajectories before they discharge on an electrode's surface.

In order to effect mass analysis using quadrupole mass analyzers, relationships between the various parameters involved in the experiment and the state of the ion (i.e., whether its trajectory is stable or unstable) must be considered. Such is provided by the Mathieu equation, a second-order differential function that allows the prediction of charged particle behavior in a quadrupole electric field [47]. With the Mathieu function, ion motion in a quadrupole mass analyzer may be determined as either stable or unstable, depending on the values of two *stability factors*, namely, a_u and q_u (shown here for a QMF)

$$a_u = \frac{8zeU}{mr_0^2\Omega^2} \tag{1.8}$$

$$q_u = \frac{4zeV}{mr_0^2\Omega^2} \tag{1.9}$$

where the subscripted u in a_u and q_u denotes the dimension (x or y), U is the DC potential (zero-to-peak), V is the RF potential (zero-to-peak), z is the number of elementary charges on an ion, e is the elementary charge (1.602×10^{-19} C), m is the ion mass [in daltons (Da)], r_0 is the inscribed radius [in centimeters (cm)], and Ω is the RF angular frequency [in radians per second (rad/s)]. Because the potentials applied to the x and y pairs of an ideal QMF or 2D QIT (and by analogy 3D QITs) are 180° out of phase, at any given instant the y-dimension parameters a_y and q_y are of equal magnitude but opposite in sign to a_x and q_x; that is, $a_x = -a_y$ and $q_x = -q_y$. The relationship between the a and q terms may be represented graphically with a Mathieu stability diagram (Figure 1.5). The boundaries of the stability diagram represent the

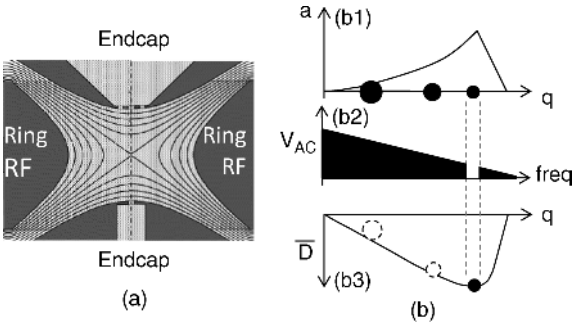

FIGURE 1.5 Depiction of some aspects of quadrupole ion traps. (a) cross section of a quadrupole ion trap, where electrodes are solid and equipotential field lines are indicated (image modified from Ref. 194, with permission of Elsevier); (b) some principles involved in mass-selective isolation: plot (b1) indicates relative positions of three ions along the q axis of the Mathieu stability diagram; plot (b2) indicates the applied waveform that resonantly accelerates and ejects all ions except those of the m/z of interest (which coincide with the waveform notch); plot (b3) depict the pseudopotential well depth, where the m/z of interest is shown in the deepest region.

set of a_u,q_u values at which an ion's trajectory transitions from stable to unstable. Although there are multiple regions of stability defined by the Mathieu function, only the region known as *region 1* is typically considered, as this region is the least demanding in terms of voltage required for ion trajectory stability (in terms of both DC and RF). The bounds of region 1 are defined as those at which the term β equals 0 or 1 for both the x and y dimensions.

Ion motion within quadrupole ion traps (QITs) are described by the Mathieu function in a manner similar to that for the QMF. However, the way in which QMFs and QITs perform mass analysis are different, owing to differences in the dimensionality of their electric fields. While QMFs can trap ions in the x/y plane, they cannot do so along the ion optical axis. In contrast, QITs have either RF or DC trapping potentials in the z dimension (for 3D and 2D traps, respectively). Geometrically speaking, a 2D trap can be created from a QMF by simply installing thin lenses at the ends of the QMF and applying DC stopping potentials to them. A 3D trap, which features RF trapping potentials in three dimensions, is typically is constructed of a toroidal *ring electrode* with two *endcap electrodes* that cover the openings at the top and bottom of the toroid.

There are several possible ways to create a mass spectrum with a QMF, but the device is usually operated in *mass-selective stability* mode, whereby a scanline is chosen on the Mathieu stability diagram, which is characterized by a constant a/q ratio. Through the course of an analytical scan, the DC and RF potentials are ramped such that only a narrow m/z range will be allowed passage through the QMF per unit time. Calibration of the a/q ramp with the detector timing allows mass spectra to be produced by plotting detected ion current versus time.

As with QMFs, there are multiple ways to perform mass analysis on a QIT. However, the most typical is that of a *mass-selective instability* [49] scan with resonant ejection; this mode features a scanline that lies along only the q axis of the stability diagram (no DC components). As ions oscillate within a trapping RF field, their travel is characterized by their secular frequencies

$$\omega_{u,n} = \pm\left(n + \tfrac{1}{2}\beta_u\right)\Omega \tag{1.10}$$

for $\omega_{u,n}$ is the secular frequency in the u dimension, n is the order of the fundamental secular frequency (typically $n = 0$), Ω is the fundamental frequency, and β_u is approximated as

$$\beta_u = \sqrt{a_u + \tfrac{1}{2}q_u^2} \tag{1.11}$$

for $q_u < 0.4$ [47]. During QIT mass analysis, $\omega_{u,0}$ is simplified as follows:

$$\omega_{u,0} = \frac{q_u\Omega}{2\sqrt{2}} \tag{1.12}$$

During QIT mass analysis, as the RF is ramped, ions acquire different secular frequencies. A low-voltage supplemental alternating-current (AC) waveform is applied to the electrodes in the dimension intended for ejection at a frequency corresponding to the desired q value at which ions are to be ejected (often between 0.7 and 0.9). As ions are scanned through this q-value, they become destabilized and are ejected through holes in an electrode for subsequent detection. By performing resonant ejection, one can scan an ion population through this "hole" of instability with the result of better resolution than can be obtained by RF-only scanning of the population through the stability boundary, which is subject to inherent instability in the mass spectrometer electronics in addition to a shallow D_u (which can cause frequency spreading of a given m/z) [50,51].

Should a quadrupole analyzer have nonlinear fields (nonquadrupolar contributions), the representation of the Mathieu stability diagram becomes overlain with internal points and lines of nonlinear resonance at which ions may be ejected or made to undergo undesired excitation [47]. In practice, QMFs and QITs are often subject to nonlinear resonances, particularly those devices that are of a simplified geometry (and hence have nonideal trapping fields). However, the addition of nonlinear resonances can also be utilized to advantage, as has been demonstrated with the rectilinear ion trap (RIT), where ions scanned through the nonlinear point at $q_x = 0.81$ were shown to have remarkably sharper peak shapes than at any other resonant frequency (Figure 1.4); this occurrence is attributed to the proximity of the RIT β_x value to the known octapolar nonlinear resonance point of $\beta = 0.7$ [50].

Finally, another way to determine trapped ion trajectory stability is to consider the pseudopotential well. The pseudopotential well is the representation of the strength of the electric field applied to the trap electrodes. At any instant, a trapped ion in a quadrupole field is at once stable in one dimension (figuratively, near the bottom of a potential "well") yet unstable in another (figuratively, near the top of a potential "hill"). In order to maintain stability, several conditions of energy must be met, including: (1) the ion kinetic energy KE_{ion} cannot exceed the pseudopotential well depth in a particular dimension D_u; (2) the RF frequency, which is 180° out of phase between electrode pairs, must alternate at a rate sufficient to ensure that the ions do not remain too long on the potential hill in the unstable dimension so as to escape the device. Paul has described the mechanical analog of the quadrupole pseudopotential as a "rotating saddle" that inverts with every 90° of phase. The Dehmelt approximation to the quadrupole pseudopotential describes the dependence of D_u on the q parameter and the RF potential in a 2D QIT [52]:

$$D_{x,y} \approx \frac{qV_{RF}}{4} \tag{1.13}$$

Consideration of D_u is important, as an ion with a kinetic energy higher than that of D_u will not be contained by that field. This is of practical consequence for matters such as ion injection, ion ejection, and various forms of ion manipulation.

1.3.3 Time-of-Flight Mass Spectrometers

The premise of separations by time-of-flight MS (TOF-MS) is that a mixture of ions of varying *m*/*z* yet the same kinetic energy will separate over time owing to differences in velocity. These differences in velocity are measured in terms of the time that it takes ions to reach a detector surface after being pulsed into a flight tube (e.g., see Figure 1.6a). The technique was first demonstrated in 1948 by Cameron and Eggers, whose instrument, the "ion velocitron," was just capable of baseline resolution between N_2^+ (28 Th) and CF_2Cl^+ (85 Th) using a 320 V acceleration potential [53]. Despite the straightforward concept of mass analysis by TOF, the field took a long time to come to its present state of maturity. Issues with minimizing distributions of kinetic energy, spatial coordinates, and angular distributions have taken decades to overcome. Spectral quality was also notably hampered by the lack of fast detection electronics. In order to achieve high-quality spectra, TOF mass spectrometers must be constructed to and operated with very high standards, including high-precision mechanical tolerances and even strict control of the flight tube material and temperature to avoid thermal expansion and the consequent variation in mass calibration. Much progress in TOF development occurred in the 1980s, when the 'biological revolution' in MS spurred interest in the development of instruments capable of analyzing high-mass samples. The coupling of MALDI ion sources with TOF analyzers became very common, as the unlimited upper mass range of TOF meshed well with the high-mass ions and pulsed-ion generation characteristic of MALDI. Through it all, TOF mass spectrometers have evolved to take their place as

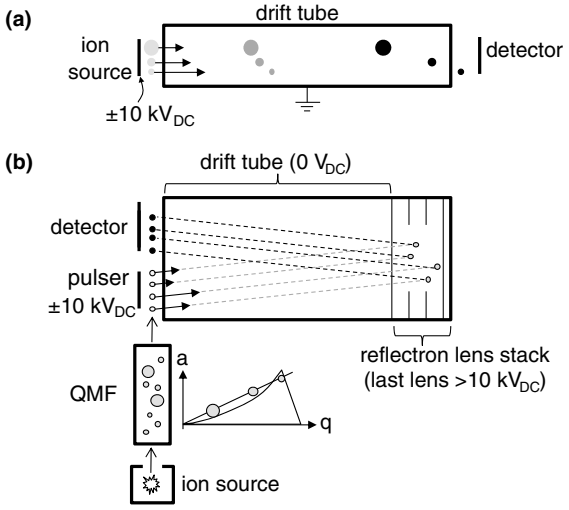

FIGURE 1.6 Two depictions of time-of-flight mass spectrometers: (a) a linear TOF arrangement where the filled circles represent ions of different masses and the arrows represent their velocity magnitudes; (b) a quadrupole TOF (Q-TOF) in which an ion beam is purified in *m*/*z* first by a quadrupole mass filter and the ions are subsequently pulsed orthogonally into a reflectron TOF.

popular instruments valued for their high resolution, mass accuracy, and sensitivity. Today, commercial TOF-based instruments are capable of providing resolutions of >10,000, mass accuracies of a few ppm, and the capability for performing MS/MS. The interested reader is referred to a few recent reviews for further details on TOF-MS than those provided here [54–59].

The TOF concept is observed in the equivalence of kinetic energy with an ion's acceleration through an electric field

$$\tfrac{1}{2}mv^2 = zeV_{\text{accel}} \tag{1.14}$$

where m is ion mass (in kg), v is ion velocity (in m/s), z is the number of elementary charges on an ion (unitless), e is the elementary charge (1.602×10^{-19} C), and V_{accel} is the potential through which the ions are accelerated (in volts). Rearrangement of this identity yields the equivalence of the mass-to-charge ratio m/z

$$\frac{m}{z} = 2zeV_{\text{accel}}\frac{1}{v^2} \tag{1.15}$$

which demonstrates that m/z scales with the inverse square of velocity. Stated another way, the TOF for an ion may be derived by substituting velocity with distance over time ($v = d/t$). By doing so and rearranging Eq. (1.15) to solve for t, we obtain

$$t = \sqrt{\left(\frac{m}{z}\right)\left(\frac{d^2}{2eV_{\text{accel}}}\right)} \tag{1.16}$$

which indicates that flight time scales with the square root of m/z, an equality that is perhaps more meaningful than Eq. (1.15) from the measurement perspective.

All TOF mass spectrometers include an ion source, a gating mechanism to initiate or stop ion introduction into the mass analyzer, a drift region in which ions of near-equivalent KE separate based on differences in velocity, a plane detector, and a high-vacuum system. The category of TOF mass spectrometers may be further subdivided into three classes (see Figure 1.6a, b): linear TOF, reflectron TOF (reTOF), and orthogonal acceleration TOF (oaTOF). The linear TOF is the first and hence "classic" design, while the latter two represent later versions that implement performance-enhancing design features. Regardless of the particular design employed or method of ion generation, TOF-MS analysis begins with the introduction of a population of ions into the region adjacent to the start of the flight tube. The ideal conditions in this region are such that the ion population has a very narrow KE spread and occupies a region of space that is narrow in the dimension of the flight tube. To inject ions into the drift tube, a high-potential DC signal is applied (example conditions: rise time = 25 ns; <1 μs duration; 1.5 kV potential) [54] at a rate of several kilohertz (kHz), thus triggering the initiation of ion flight into the field-free drift tube (no further acceleration occurs in this region). Within the drift tube (often 1–2 m in length), ions will travel with kinetics defined by their acceleration potential [typically a few kiloelectronvolts (keV) to several tens of keV] with KE spreads within a several tens

of millielectronvolts (meV) or better (depending on the source type and instrument quality). Within the drift region, ion separation is based on differences in velocity, with ions of low *m*/*z* traveling with the greatest speed. Detection of ions occurs at a planar detector, which records signal intensity versus the time since the injection pulse was triggered.

The optimization of TOF construction and operation has proved critical to achieving high-quality data in terms of resolution, sensitivity, and duty cycle. Three important advances made at the TOF source region were those of time lag focusing (for gas-phase ions) [60], delayed extraction (DE, a time lag focus analog for linear MALDI-TOF) [61,62], and the advent of orthogonal acceleration TOFs. The principle of timelag focusing as well as delayed extraction is centered on correcting space and velocity distributions at the analyzer source, that is, correction of the kinetic energy disparity arising from ions initially moving in a wide distribution of velocities and directions in the moments shortly before injection into the drift tube. To minimize this directional disparity, rather than triggering ion injection into the drift tube immediately after an ion population enters the source region, a tunable time delay (μs timescale) may be employed to allow the ions to expand over a wider distance (a few mm) in the dimension of the flight tube. Then, when a potential is applied to accelerate ions into the drift region, the ion population will have expanded across a greater distance along the dimension of the flight tube; the end result is such that the ions nearer the rear of the source volume will be accelerated for a longer time than will the ions nearer to the drift tube. Provided an appropriate time delay is employed, the "lagging" ions of a particular *m*/*z* range can be made to "catch up" with the leading ions and hence enhance spectral resolution. Another way in which spatial distributions in the analyzer source are minimized is through *orthogonal acceleration*. Mass spectrometers that feature orthogonal acceleration have the ionization occur in a region distinct from the analyzer, forming a beam that will ultimately travel transverse to the flight tube axis. Often, these beams are collisionally damped at moderate pressures to minimize kinetic energy distributions as well as beamwidth (including spatial distribution in the dimension of the flight tube), which may be further narrowed by slits whose smallest dimension is parallel with the flight tube axis. Hence, oaTOFs allow the sampling of a quasiplanar beam. Because the ions have a velocity component transverse to the flight tube, the detector may need to be shifted so that the center of the TOF source and the detector are not co-axial. It should also be noted here that the use of RF multipoles in oaTOFs permits the storage of the ion beam (via trapping) during the period in the TOF cycle when ions are not pulsed into the flight tube; hence, oaTOF designs are one way in which TOFs achieve a high duty cycle (between 5% and 100%) [59].

In addition to instrumental advances at the TOF source, TOF performance was also improved by correcting dispersions at one or multiple points within the ion flight path using a reflectron (or ion mirror). The idea for the reflectron originated from Mamyrin in the early 1970s when he was reminiscing on childhood games in which the objective was to see who could throw a ball the highest [58]; in such a game, the highest-thrown ball traveled with the greatest initial and final velocity, yet it also necessarily spent the most time decelerating at the apex of its arc before its return trip

to Earth. From this concept was born the TOF equivalent, the "ion mirror," a stack of grids or annular disks to which is applied static DC potentials such that ions may penetrate the field to varying depths dependent on their kinetic energy. As the mirror potential is ultimately higher than all ion kinetic energies, the result is that each ion entering it will decelerate, arrest its forward motion, and then reaccelerate away from the mirror, eventually achieving the same velocity at which it entered the mirror. Since the highest-KE ions penetrate the mirror to the greatest depths, they must necessarily spend the most time in the mirror; in effect, this allows lower-velocity ions of the same m/z to travel a shorter distance through the mirror before returning to the drift region on the way to the detector (or another ion mirror). The end result is a narrowing in flight time distributions for ions of a given m/z (higher resolution; e.g., while commercial linear TOFs may provide $R \sim 1000$, commercial reTOFs are capable of $R = 7{,}500$–$20{,}000$) [43]. The reflectron is also a convenient way to effectively lengthen the drift tube length while allowing an instrument to have a smaller footprint.

The detector and data acquisition elements of TOFs have been subjected to marked improvements coinciding with the development of fast digital electronics. Since TOF analysis requires ions to travel at several tens of keV for optimal resolution, sensitivity, and duty cycle, the signal acquisition must accommodate time resolution on a very short timescale (ns range); should detection time resolution be slower than the arrival time distribution of a peak, the spectral resolution is then limited by the detector. Hence, conventional TOF detectors [microchannel plates or (MCPs); essentially a thin planar detector with thousands of continuous-dynode channels on the scale of tens of μm in diameter] [63] as well as signal processing circuits [time-to-digital converters (TDCs)] must characteristically have ultralow intrinsic signal delay. Fortunately, most MCPs and TDCs used in modern instrumentation are capable of operation with sub-nanoscale time resolution.

1.3.4 Fourier Transform Ion Cyclotron Resonance Mass Spectrometers

The history of ion cyclotron resonance MS (ICR-MS) begins in the 1930s when Lawrence and coworkers developed the theory and early instrumentation for cyclotrons [64,65]. Cyclotrons are instruments capable of trapping and manipulating ions under high vacuum in a strong magnetic field, in which ions move with a circular trajectory on a plane perpendicular to the magnetic field (see Figure 1.7a). Cyclotron research has long focused on aspects of atomic physics that require ions to be accelerated to very high energies. For example, cyclotrons are used for the bombardment of atomic ions to induce transmutation—the formation of one element as a fission product of a heavier element; such research allows the production of rare unstable isotopes suitable for scientific or medical interests. As early as 1949, the potential for measuring mass using cyclotron principles was recognized by Hipple, Sommer, and Thomas, who constructed the first cyclotron mass spectrometer (termed the *omegatron*). In the omegatron, ions were induced by a low-voltage resonant AC frequency to gradually expand their orbital paths along a plane orthogonal to a

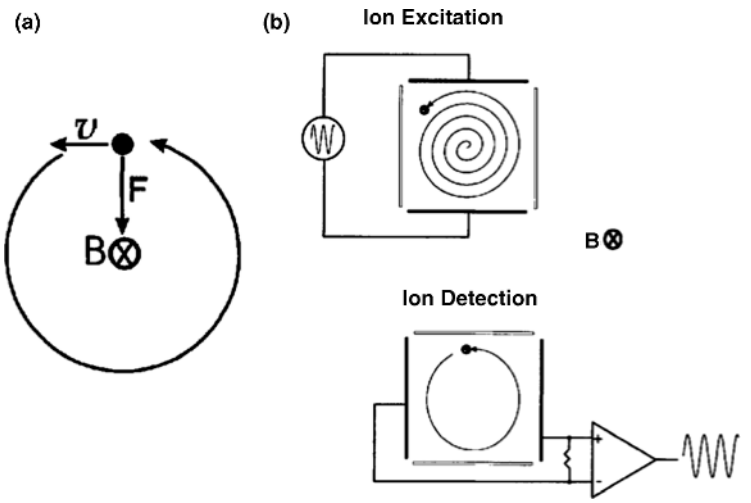

FIGURE 1.7 (a) If an ion in motion (indicated by arrow with velocity vector *v*) experiences a magnetic field in a dimension orthogonal to the ion motion (as indicated by the tickmark x), the ion will experience an inward force that causes circular motion in the plane transverse to the magnetic field lines; (b) depiction of ion excitation to the detection radius followed by transient image current detection (both diagrams reprinted from Ref. 69, with permission of John Wiley & Sons, Inc.).

magnetic field; this resulted in the radii of the excited ions' orbits expanding until impact occurred with an electrometer electrode [66]. The earliest efforts were focused on studying low-mass particles and their properties, with results including the baseline resolution of deuterium and diatomic hydrogen ions, which differ in mass by just less than 0.002 Da [66,67]. With the incorporation of *image current* detection in 1965 by Wobschall, ions could be detected nondestructively via the differential amplification of current flowing through a circuit connecting opposing electrodes as ion packets passed by them one at a time; hence, image currents allowed higher signal intensity and lower sample consumption [68]. Many early ICR-MS applications involved ion–molecule reaction studies, but the technique was hindered for broader applicability by the necessity of scanning the magnetic field over several tens of minutes to acquire a mass spectrum at unit resolution [69,70]. In 1974, Comisarow and Marshall published their conception of an ICR mass spectrometer that was capable of the simultaneous detection of multiple *m*/*z*, a development that allowed ICR mass spectrometers to acquire spectra in $\frac{1}{100}$th the time of conventional methods [71,72]. To perform the Fourier transform technique, all ions comprised within a broad *m*/*z* range were excited to the detection radius and simultaneously detected as a complex signal in the time domain, which could then be processed by Fourier transform (FT) for conversion to the frequency domain and then subsequent conversion into the *m*/*z* domain via application of a calibration function. Today, FT-ICR MS is used for many applications requiring the ultimate mass spectrometric performance in terms of resolution and mass accuracy; one good example is the detection of protein

ions generated by electrospray ionization (ESI), for which FT-ICR is capable of resolving the isotopes of species having masses >100 kDa while allowing assignment of the accurate molecular mass to within 3 Da [73,74]. Routine figures of merit include single-digit ppm mass accuracies and resolving powers of 10^6–10^4 (for a typical 1 s mass spectrum over the m/z range up to 1000 Th) [73]. For further insight into the workings of ICR MS beyond the introductory level presented here, the interested reader is referred elsewhere for several excellent and much more detailed reviews [41,69,70,73–75].

Ion cyclotron resonance mass spectrometers are built around their magnet, with the geometry of the analytical cell chosen depending on the type of magnet used; permanent magnets and some electromagnets operate with cubic geometry so that the magnet poles might face each other to produce a homogenous field, while the highest field strengths are achieved with solenoidal superconducting magnets that are typically paired with coaxially oriented open-ended cylindrical cells [69,73]. Ion cyclotron instruments incorporate a balance of attractive and repulsive forces that causes ion motion to describe a circular path on a plane orthogonal to the magnetic field. Magnetically induced ion motion in this plane is due to a balance of centripetal (inward-drawing) and centrifugal (outward-drawing) forces, as can be seen in the following identity:

$$qvB = \frac{mv^2}{r} \tag{1.17}$$

Here q is the product of the elementary charge (e) and the number of elementary charges (z), B is the magnitude of the magnetic field, m is ion mass, v is ion velocity, and r is the orbital radius. By application of a low-amplitude RF excitation signal in one dimension of the orbital plane, ion trajectories can be made to spiral outward as the ions gain kinetic energy (see Figure 1.7b). When ions reach the detection orbit, the excitation signal is turned off and the ions travel along the detection orbital radius. By substituting angular frequency ($\omega = v/r$) into Eq. (1.17), the cyclotron frequency (ω_c) may be characterized as

$$\omega_c = \frac{q}{m}B \tag{1.18}$$

A remarkable quality of the cyclotron frequency is that it is independent of ion kinetic energy—where two ions of the same m/z to have different energies, the end result would be only that the one of higher energy (and hence orbital radius) would travel nearer to the detection electrodes and create a relatively larger detection signal. Hence, with no need for energy focusing, ICRs have an inherent advantage over other mass analyzers in their capability to produce spectra with high resolution.

In addition to ion cyclotron motion in the cyclotron plane (the x–y plane), ions within an ICR cell typically also experience two other types of field-induced motion. The first is motion in the axial (z) dimension, which is due to a low-voltage electrostatic trapping field that is maintained for the duration of an MS experiment. Hence, as ions precess in their cyclotron orbits, they will also oscillate in the axial

dimension to a small extent. The other motion an ion experiences is that of *magnetron motion*, a consequence of the magnetic and electric fields acting on ions in orthogonal directions. Magnetron motion arises because the radial electrodes (one pair each of excitation and detection electrodes) are grounded while the *z*-dimension "trapping" electrodes are of equal potential; hence, the midpoint between the trapping plates have some nonzero potential and a net force is directed radially outward toward ground [69]. Consequently, magnetron motion causes a minor localized spiraling trajectory in ion motion as the ions travel on the cyclotron orbits, which are of much higher magnitude. Magnetron motion is typically of a much lower magnitude and frequency relative to axial motion, which in turn is of a much lower magnitude and frequency relative to cyclotron motion [41]. Since it is generally undesirable, magnetron motion is effectively controlled by minimizing the axial ion velocity.

A unique aspect of FT-MS is that it allows detection of all ions over a broad *m*/*z* range via image current, whereby the differential amplification of current in the circuit that links the two detection electrodes results in a time-domain signal representative of the cyclotron frequency. By detecting ions in a nondestructive manner, each ion may be detected many times, enabling enhanced signal-to-noise ratio (S/N) as well as reduced sample consumption. In order to allow detection of all ions pseudosimultaneously, they must all be at about the same radius within the ICR; such a condition is made possible through stored waveform inverse Fourier transform (SWIFT). Developed by Marshall and coworkers, SWIFT involves the calculation of a waveform in the frequency domain followed by its inverse Fourier transform into the time domain, with the result that all ions of interest will be excited to the same radial amplitude through application of the SWIFT waveform [76]. Previous methods of broadband excitation, such as chirping (a rapid scan through all frequencies), lead to undesirable dispersions in orbital radius, which makes accurate relative abundances difficult to determine. The resultant multifrequency image current signal is processed by Fourier transform from the time domain into the frequency domain, from which a conversion to *m*/*z* may be done on the basis of preexisting calibration data [71,72].

1.3.5 Orbitrap Mass Spectrometers

The Orbitrap mass analyzer is an "evolved" version of the Kingdon ion trap that contains ions in an electric field between a coaxial pair of electrodes. The Kingdon trap, originally conceived in 1923 by K. H. Kingdon [77], consists of an electrostatic trapping potential defined by the logarithmic field between a cylinder and a wire that it surrounds; ion confinement is achieved when the electrostatic attraction between ions and the central electrode (centripetal force) is countered by the ion motion in the direction tangential to, and hence away from, the center electrode (centrifugal force). The balanced relationship between centripetal and centrifugal forces in the Kingdon trap may be observed as [77]

$$qV = \frac{1}{2}mv^2 \cdot \left(\frac{R}{r}\right) \tag{1.19}$$

where q is the product of the quantity of elementary charges and the elementary charge ($q = z \cdot e$, for z is a unitless integer and e is 1.602×10^{-19} C), V is the electric potential, the ion kinetic energy $\frac{1}{2}mv^2$ consists of mass (m) and velocity (v) components, R is the radius of the outer electrode, and r is the radius of the inner electrode. As a consequence of the centripetal and centrifugal forces being balanced, an ion that is stably trapped will assume an elliptical orbit about the wire with its eccentricity (degree of elliptical vs. circular orbit character) depending on the field potential, the ion kinetic energy, and the ion's angle of approach. To contain ions in the axial dimension of a Kingdon trap, repelling potentials are applied to electrodes located at both ends of the cylinder.

Kingdon traps have been used for a variety of purposes, including the study of ions by optical spectroscopy and development of the orbitron ion pump [78,79]. The first application of a Kingdon trap as a mass analyzer occurred in 1981 when R. D. Knight created a modified-geometry Kingdon trap that had no endcap electrodes and an outer electrode that was tapered at both ends and bisected at its middle, a geometry that provided an approximately quadrupolar field in the axial dimension [80]. Knight used his trap to monitor the image current produced on the bisected outer electrodes by the near-harmonic oscillation of ions in the axial dimension, allowing him to perform mass analysis on plasma species generated by laser ablation of various metals [80]. However, field nonidealities in this simple cylinder-about-a-wire geometry caused an undesired interdependence of ion motion between the axial dimension and the radial plane, inhibiting truly harmonic oscillations (and hence spectral quality) and prompting the development of an "ideal" electrode geometry (i.e., the Orbitrap) to provide a purer axial quadrupole field; of anecdotal interest, this is the opposite trend of the developments in the RF ion trap community, which began with ideal geometries (of hyperbolic shape) and later branched out to simplified versions [e.g., the cylindrical ion trap (CIT) [81] or the rectilinear ion trap (RIT) [50]] when it was determined that performance for those devices was not severely worsened by implementing simpler fabrication procedures.

In 2000, Makarov created a "Knight-style Kingdon trap" (the Orbitrap), which featured an electrode geometry allowing a near-ideal quadrupole field along the axial dimension [82]. Rather than a cylinder-about-a-wire geometry faced with endcap plates (as for the Kingdon trap), the Orbitrap geometry consists of an outer "barrel-like" electrode, which is tapered near its ends, in addition to a "spindle-like" center electrode, which is also tapered at its ends yet broadened at its middle (see Figure 1.8). With its outer electrode actually split into two isolated electrodes at the equatorial axis ($z = 0$), the Orbitrap is able to perform differentially amplified image current detection using the outer electrode pair in lieu of the endcap plates of previous designs. The quadrologarithmic potential of the Orbitrap, $U(r,z)$, is the sum of a quadrupolar field with that of a cylindrical capacitor, and is defined as [82]

$$U(r,z) = \frac{k}{2}\left[\left(z^2 - \frac{r^2}{2}\right) + R_m^2 \cdot \ln\left(\frac{r}{R_m}\right)\right] + C \tag{1.20}$$

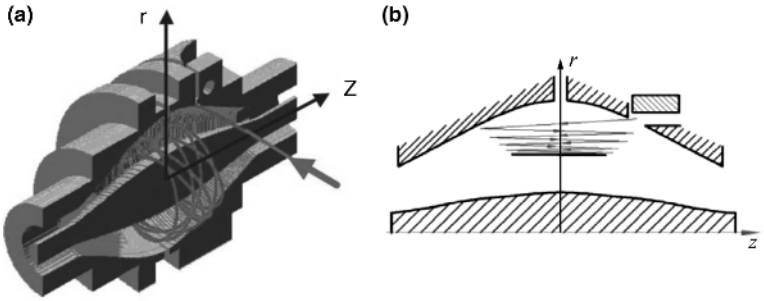

FIGURE 1.8 (a) Isometric cutaway view of the Orbitrap mass analyzer; (b) cutaway view of axial ion trajectory at injection and during electrodynamic squeezing (both diagrams reprinted from Ref. 78, with permission of John Wiley & Sons, Inc.).

where r and z are cylindrical coordinates, k is field curvature, R_m is the characteristic radius, and C is a constant. An important consequence of Orbitrap geometry is that trapped ion motion along the axial (z) dimension is independent of ion kinetic energy, the angle of the orbit with respect to the z axis, and spatial spread of the ion population in the radial (r) plane (as indicated by the absence of rz cross-terms in the potential). Detection on an Orbitrap analyzer occurs through differential amplification of the image current induced in the two outer electrode halves, which are bisected at the $z = 0$ plane. The shape of the Orbitrap electric field is such that ions moving axially are trapped in a quadrupolar potential well and hence their axial motion is sinusoidal in nature with a characteristic frequency dependent on m/z, as described in the following relationship:

$$\omega = \sqrt{k\frac{z}{m}}$$

Here ω is ion axial frequency and k is a constant of the axial restoring force. It is interesting to note that resolution ($R = m/\Delta m$) for an Orbitrap decays with an inverse-root relationship with m/z; hence, for all except the highest-field-strength FT-ICRs and for analyses of practical timescales ($\sim$1 s), the Orbitrap has superior performance at and above m/z of moderate value (i.e., 2000 Th) [79]. To measure mass-to-charge ratio (m/z) on the Orbitrap, the frequency of ion motion in the z dimension is measured as an image current by the split outer electrodes and then fast-Fourier-transformed into a frequency spectrum, from which a mass spectrum can be obtained after accounting for m/z calibration. Since the image current method of detection does not destroy ions, they are each detected many times during a given analysis, and hence less sample may be consumed per spectrum relative to "destructive" techniques.

Ions must be introduced into an Orbitrap mass analyzer with stable trajectories of narrow distribution along the z axis to ensure the highest spectral quality. To ensure that this occurs, several conditions must be met: (1) the Orbitrap must be operated at high vacuum (2×10^{-10} mbar) to avoid energy and trajectory-dispersive

ion–molecule collisions, (2) ions must be injected within a narrow spatiotemporal window (i.e., at high kinetic energy), and (3) the Orbitrap potential must be ramped during ejection in a process termed "electrodynamic squeezing" to ensure that a wide mass range is captured (see Figure 1.8b). Narrow spatiotemporal ion injection is facilitated by collisional cooling in a storage multipole just outside the Orbitrap in addition to rapid pulsing ($\sim$100–200 ns; kinetic energies $>$1 keV) of the ions between the storage mutlipole and the Orbitrap entrance [78]. Electrodynamic squeezing is a method whereby the center electrode amplitude is increased during the period of ion injection ($\sim$20–100 μs) so that the ions may be injected tangentially to the outer electrode surface yet avoid discharge on the outer electrode through constriction of their orbital radii [82]. An additional requirement of injection is that the ions be introduced at a position offset from $z = 0$ such that they may be induced into harmonic oscillations via their introduction on one side of the quadratic potential well.

The most impressive attributes of the Orbitrap are its resolution and mass accuracy capabilities, which rival those of FT-ICR for many practical applications. Resolution on an FT mass spectrometer depends on the total acquisition time, but typically mass spectrometers are expected to provide about one spectrum per second for practical reasons (e.g., online chromatography) [75]. Orbitrap data that last for one second have been shown to yield a resolution of $>$100,000 for m/z 400 [83]. The Orbitrap is currently capable of acquiring data for up to 1.8 s before the transient signal fades away as a result of packet decoherence [79]. The limitation to extended data acquisition times on the Orbitrap is that the axial ion phase will become decoherent and hence meaningful signal will not be achieved. The mass accuracy on an Orbitrap is generally $<$5 ppm if externally calibrated or $<$2 ppm with internal calibration; optimized mass accuracies of 0.2 ppm have been demonstrated [79]. The dynamic range of mass accuracy has been shown to be about 1 : 5000 [83], meaning that an ion species present at a very low signal will be ascribed the same m/z as that same species were it to be present as a population of 5000 $\times$ greater abundance; this is a testament to the low susceptibility of the Orbitrap to space charge influences.

In commercial embodiments of Orbitrap mass spectrometers, the analyzer is located behind a two-dimensional quadrupole ion trap (2D QIT) [84]. The presence of the 2D QIT allows for a variety of advantages that cannot be achieved by the Orbitrap alone. Most notably, tandem MS (MS/MS) may be performed "upstream" in the 2D QIT prior to introduction of isolated species or product ions for high-resolution/accurate mass analysis in the Orbitrap. Fittingly, automated workflows have been developed to allow simultaneous analyses on both analyzers for the purpose of high-throughput analyses for which the LTQ-Orbitrap™ (where LTQ = linear trap quadrupole) is employed.

1.4 TANDEM MASS SPECTROMETRY

Tandem MS is the practice of using multiple stages of ion manipulations, including m/z isolation and fragmentation. Tandem MS is also referred to as "MS/MS" for two

stages of mass analysis or "MS^n," where n is the number of stages of mass analysis. The benefits to MS^n include the following: (1) increased signal-to-noise by reduction in chemical background peaks, (2) the capacity for purifying a mixed ion population to provide an isolated reagent species for reactions, and (3) enhanced chemical specificity in terms of structural analysis when employing strategies of fragmentation.

The isolation and fragmentation of analyte ions for the purpose of structural analysis is the most common application of MS^n. A mass spectrometrist can use an ion activation technique to provide detailed structural characterization of ions by allowing the attribution of both molecular and fragment peaks to a particular chemical species. For example, single-stage mass analysis of the protonated form of caffeine [molar mass = 194.2 Da] will provide only the m/z of the intact precursor. Since unknown chemical species are seldom identified with such limited information, it can be extremely difficult for the analyst to determine the most probable structure without knowledge of the fragment masses and an interpretation of the intramolecular connectivity. This is particularly true for any chemical system with more than a few atoms when measured on an instrument that cannot accurately determine the exact mass (from which the elemental composition can be derived) to good precision (such is typically the case for ion traps). However, if the analyst were to first isolate the unknown species and then induce fragmentation, clues about the ion structure will be provided according to the m/z and relative abundances of the product such that relatively low-resolution instruments can suffice for accurate structural identification.

There are a variety of means by which ion activation may be achieved, including interactions of the analyte ion with neutral molecules, surfaces, electrons, photons, electric fields, or other ions. The most commonly applied method for activation is *collision-induced dissociation* (CID), in which ion–molecule collisions result in characteristic fragmentation of the precursor ion. The technique known as *surface-induced dissociation* (SID) [50,85] involves the collision of precursors with a surface such that the resultant product ions are similar to those arrived at by CID. Electron-induced dissociation techniques, such as electron capture dissociation (ECD) [37] and electron transfer dissociation (ETD) [38,86], involve interactions between ions and free electrons or between ions of opposite polarity, respectively, which leads to radical-driven fragmentation which yields product ion information that is often complementary to CID. Depending on the specific technique applied, photoionization techniques can involve photoabsorption to provide thermodynamically favored product ions [e.g., infrared multiphoton dissociation (IRMPD) [87]] or even field ionization by high-power ($>10^{14}$ W/cm^2) femtosecond lasers [88]. For brevity and relevance to the audience of this book, the following discussion of ion activation is focused on three techniques that are commercially available: CID, ECD, and ETD.

1.4.1 Ion Isolation

Prior to target ion fragmentation, it is common to perform an isolation step so that no interfering species remain to hamper spectral interpretation. Most mass spectrometers

of the trapping type (QITs and ICRs) are capable of performing *tandem-in-time* MS^n as sequential operations in a single analyzer. Quadrupole ion trap and FT-ICR isolation is achieved by application of notched broadband AC waveforms, which permits the ejection of all ions except those that are desired to maintain stable trajectories [73]. The notable exception for on trap MS/MS capability in is the Orbitrap, which cannot practically implement MS/MS for structural analysis without destabilizing precisely controlled ion trajectories; however, a workaround to this problem has been developed by coupling the Orbitrap with an upfront ion trap to perform preselection and any necessary fragmentation [84]. The remaining analyzer types (magnetic sectors, quadrupole filters, and TOFs) require *tandem-in-space* configurations, where two or more analyzers are used; the typical setup involves a first analyzer performing the target ion selection and a second analyzer performing the analysis, with an intermediate "collision cell" in place to effect the activation. Magnetic sectors can perform target ion isolation by adjustment of field strengths such that only the m/z of interest can be passed through a narrow slit and onward to a collision cell or/and the next stage of mass analysis. Isolation in quadrupole filters is achieved by application of constant a (DC) and u (RF) values to the rods such that only a particular range of m/z maintains stable trajectories. TOF-MS/MS can be accomplished by placing a collision cell in the ion flight path and gating the cell open or shut depending on which ions are intended to pass into it and fragment; TOF mass spectrometers are also often arranged as Q-TOF platforms so that precursor isolation is effected within the quadrupole.

1.4.2 Ion-Molecule Collisions and Collision-Induced Dissociation

As MS is never performed in a perfect vacuum (except for some computer simulations), the presence of background gases will affect the instrument performance and in certain cases can assist in particular processes (i.e., collisional activation, thermal cooling, or directional velocity damping). Collisional processes between an ion and neutral commonly occur in all except the highest-vacuum instruments, with the frequency of collisions being determined by the *mean free path*, (λ) [41]

$$\lambda = \frac{kT}{\sqrt{2}P\sigma} \tag{1.21}$$

where λ is in units of centimeters, k is the Boltzmann constant ($k = 1.381 \times 10^{-21}$ J/K), T is temperature (in kelvins), P is pressure (in pascals; 1 Torr = 133.3 Pa), and σ is the collision cross section (in m^2) with an area represented by $\sigma = \pi(r_i + r_n)^2$ where r_i and r_n are the molecular radii of the participating ion and neutral, respectively. The collision between an ion and a neutral in free space has the center-of-mass (COM) energy E_{COM}

$$E_{COM} = \frac{1}{2}\frac{m_i m_n}{m_i + m_n} v_R^2 \tag{1.22}$$

where m_i is the ion mass, m_n is the neutral mass, and ν is the relative velocity of the two particles. When accelerated through an electric or magnetic field, KE_{ion} often becomes considerably greater than $KE_{neutral}$, which is probably at thermal energy ($\frac{3}{2}kT \approx 0.04$ eV for $T = 293.15$ K). In such an instance, the energy brought to the collision is practically wholly brought by the ion while that brought by the neutral can be ignored as follows

$$E_L = \tfrac{1}{2} m_i v_R^2 \tag{1.23}$$

where E_L, the "laboratory energy" involved in the experiment, is defined as the kinetic energy of the incident ion. Substitution of the ν_R^2 term from Eq. (1.23) in Eq. (1.22) yields the following formula:

$$E_{COM} = E_L \frac{m_n}{m_i + m_n} \tag{1.24}$$

Hence, the maximum energy available for uptake by the ion is essentially proportional to the ion kinetic energy times the quotient of the neutral mass over the summed mass of the neutral and ion. For example, Eq. (1.24) can be used to compare the energy available for uptake by an ion in the case that it undergoes collisions with He [nominal mass = 4 Da (Where u is the universal mass unit, used to express both atomic and molecular masses)] versus Ar (nominal mass = 40 Da). For an ion of m/z 100 with, say, 20 eV KE, a collision with helium will result in as much as $(20 \times 4/104) = 0.77$ eV being taken up as ion internal energy IE_{ion}. Compare this with the collision of the ion with argon: $20 \times 40/140 \simeq 5.71$ eV. With a greater relative energy uptake per collision, fewer collisions are necessary to achieve fragmentation when argon is the neutral, which exemplifies why higher-mass neutrals are often used in reaction cells in which an ion has a very limited probability of participating in multiple collisions. Two practical consequences of the choice of buffer gas can be considered in terms of analytical resolution and transfer efficiency. Consider the case of a quadrupole where the RF ramp of mass-selective instability mode is occurring, and ions are being sequentially ejected according to their m/z. Suppose that a population of ions of the same m/z are experiencing resonant excitation; they are perhaps 10 cycles from be ejected, enough time for a collision to occur with a background neutral gas atom or molecule. Naturally, the ions will eject over a distribution of times owing to their differences in position, trajectory, and velocity. However, if some ions also undergo a collision with a He atom shortly before ejection, they may perhaps lose enough KE (by conversion to IE_{ion}) to eject a cycle or two later than expected, causing a bit broader distribution of peak width. However, if the analyte ions instead collide with N_2, they could assume a still broader distribution of position/trajectory/velocity and subsequently eject over an even longer time period (poorer resolution than the He case). On beam-type instruments, a collision gas must be chosen that is of sufficient mass to promote efficient fragmentation on the timescale of ion passage through the collision cell, yet of a mass not so high as to cause excessive beam dispersion and loss of transfer efficiency (this is, of course, dependent on the incident ion kinetic energy).

1.4.3 Electron Capture Dissociation and Electron Transfer Dissociation

Electron capture dissociation (ECD) was developed in the McLafferty group in 1998 following an accidental discovery that low-energy electrons ($< 10\,\text{eV}$) captured by multiply charged peptide ions trapped in an ICR cell can induce unique fragmentation of the peptide ions [89,90]. A general chemical equation for the ECD process can be written as follows:

$$[\text{M} + n\text{H}]^{n+} + \text{e}^- \rightarrow ([\text{M} + n\text{H}]^{(n-1)\cdot +})_{\text{transient}} \rightarrow \text{fragments}$$

Since charge reduction of the precursor ions is involved, multiply charged (very often protonated) analyte cations formed by electrospray ionization (ESI) are employed in order to detect fragment ions in the ECD process. Low-energy electrons are produced with a filament-based electron gun and injected into the ICR cell at relative low energy for reaction with analyte cations [91]. Distinct from the collisional activation process, in which part of the kinetic energy is transfered to the internal energy for activation, the recombination energy between the electron and the cation causes the subsequent excitation and fragmentation. Since an odd-electron species is formed with the electron capture, ion fragmentation in ECD is majorly driven by radical chemistry [92]. Taking the multiply protonated peptide ions as an example, the normally strong N–C_α backbone bonds are cleaved homolytically in ECD, producing a complementary pair of *c* and *z* fragments as indicated in Figure 1.9a, while *b*- and *y*-type fragment ions are typically observed in CID as a result of the heterolytic cleavage of the amide bonds as shown in Figure 1.9b [93]. Note that the peptide fragmentation nomenclature follows the definition proposed by Roepstorff and Fohlman [94].

There are several unique features of ECD for the analysis of biomolecules, especially for peptides and proteins. As compared to CID, sequence analysis by ECD tends to have a smaller dependence on protein sequence and gives good sequence coverage by inducing widespread cleavages along the backbone with the exception of cleavages *N*-terminal to proline residues (owing to the residue's cyclical structure). Such nonspecific fragmentation is especially useful for identification of unknown peptides and proteins, where extensive fragmentation is required to facilitate identification of the molecular structure. Since disulfide linkages can be cleaved on electron capture, ECD has also been proved useful in characterizing peptides and proteins that contain disulfide bonds [95]. Another very attractive feature of ECD is that labile post-translational modifications (PTMs) are often preserved, such as glycosylation, phosphorylation, and sulfonation, whereas in CID they are preferentially cleaved. This feature allows not only sequence identification but also pinpointing of the location of the modification [96].

Because of the requirement of storing cations and electrons in overlapping space simultaneously, implementation of ECD is generally limited to Fourier transform ion cyclotron resonance mass spectrometers, which have the capacity to stably trap electrons. In 2004, Hunt's group demonstrated that ion/ion electron transfer gave rise

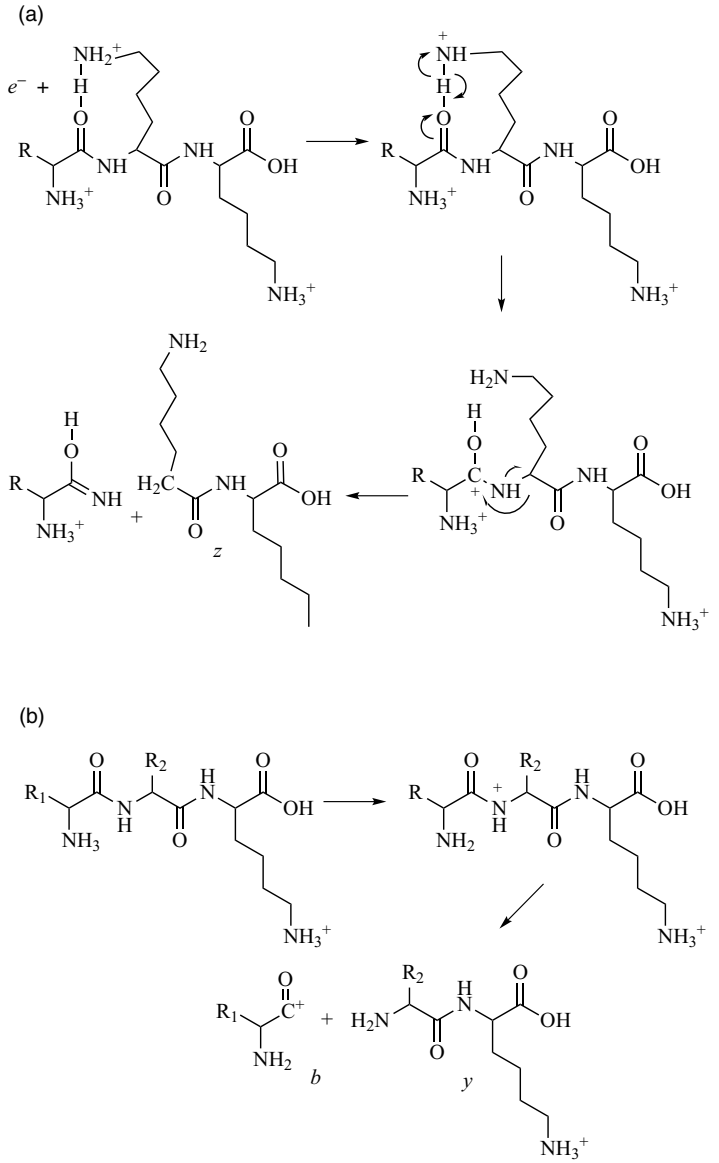

FIGURE 1.9 (a) Fragmentation scheme for production of *c*- and *z*-type ions after reaction of a low-energy electron with a multiply protonated peptide; (b) fragmentation scheme for the production of *b*- and *y*-type ions by CID of a multiply protonated peptide (both schemes reprinted from Ref. 93, with permission of the National Academy of Sciences USA).

to dissociation behavior very similar to that observed with ECD [93,97]. This dissociation process was termed *electron transfer dissociation* (ETD). ETD involves reactions between multiply charged cations and singly charged anions:

$$[\mathrm{M}+n\mathrm{H}]^{n+}+\mathrm{Y}^{-}\rightarrow([\mathrm{M}+n\mathrm{H}]^{(n-1)\cdot+})_{\text{transient}}+\mathrm{Y}\rightarrow\text{fragments}+\mathrm{Y}$$

The reagent anions selected for ETD typically have high probabilities for transferring electrons to cations; what's more, such reagent anions should also have a low probability of abstracting protons from the cations [98]. Currently, the most commonly used reagents include fluoranthene and azobenzene, the negative ions of which can be produced by chemical ionization (CI) [93] or atmospheric-pressure chemical ionization (APCI) [99]. ETD can be conducted on conventional quadruple ion traps, which are readily accessible; because of a higher pressure in QITs, good reaction efficiencies are typically obtained in relatively short times (tens of ms), allowing the coupling of the activation technique with online liquid chromatography [93]. Figure 1.10 shows the tandem mass spectra obtained from a phosphopeptide eluted during a *n*HPLC/MS/MS experiment [100]. In the ETD tandem mass spectrum (Figure 1.10b), every single backbone cleavage product is observed. The sequence can be easily assigned as RKpSILHTIR. The CID tandem mass spectrum of the same peptide (Figure 1.10a), however, is dominated by a single peak corresponding to the loss of a phosphoric acid moiety. No peptide backbone cleavage is observed, and the sequence identification is impossible.

Both ECD and ETD are still in early stages of development by any standards. This is exemplified by the ongoing debates on the mechanisms behind ECD and

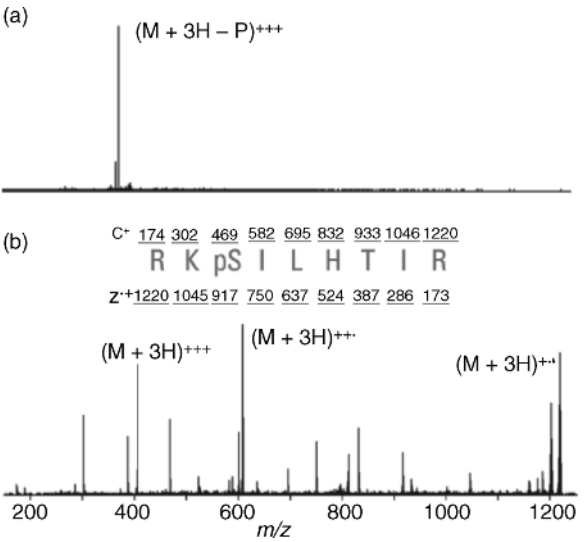

FIGURE 1.10 (a) CID and (b) ETD tandem mass spectra recorded for the phosphopeptide RKpSILHTIR (Reprinted from Ref. 100, with permission of the American Chemical Society).

ETD [101,102]. Nevertheless, the unique features of ECD and ETD guarantee them as a new category of tandem mass spectrometric technique with potentials in a variety of applications. With the launch of several commercial tandem mass spectrometers that are capable of ECD or ETD, a much wider impact of these techniques on the analysis of complex mixtures can be foreseen.

1.5 SEPARATION TECHNIQUES COUPLED TO MASS SPECTROMETRY

1.5.1 Gas Chromatography–Mass Spectrometry

During the late 1950s and early 1960s, significant advances in gas chromatography (GC) were made, allowing the technique to become one of the most prominently used in modern analytical chemistry. Early work by Martin and Synge used two liquid phases (liquid–liquid partition chromatography) to separate acetyl derivatives of amino acids [103]. Although theoretical advantages of replacing one of the liquid phases with a gaseous phase were noted, the practical application of gas–liquid partition chromatography was not reported until 1952 [104]. The same group also reported gas–liquid partition chromatography for the separation of ammonia and methylamines, as well as for the separation of volatile aliphatic amines [105,106]. Perhaps one of the greatest advances in GC instrumentation occurred in the late 1950s when Golay developed open tubular (capillary) columns [107]. Although not realized at the time, the development of these columns would make coupling of GC with MS considerably simpler in later years.

Although GC instrumentation was still in its infancy in the late 1950s, the first GC-MS instruments were actually reported around this time [25,108,109]. The "hyphenation" of the two techniques was an important advance in exploiting the benefits and minimizing the limitations of each instrument. While gas chromatography is highly efficient for the separation of complex mixtures, definitive identification of sample components is not possible with only the retention time from the chromatogram. In MS, definitive identification is possible, based on the fragmentation pattern of the molecule. Thus, MS offers highly sensitive detection, as well as structural information for each sample component separated by GC.

In one of the first GC-MS instruments reported, a conventional gas–liquid partition gas chromatograph was coupled with a time-of-flight (TOF) mass spectrometer [108]. The gas chromatograph contained four columns, the ends of which fed into a block that also contained two exit lines: one feeding into the mass spectrometer and the second feeding into a thermal conductivity detector that was used to continuously monitor the effluent. The mass spectrometer was slightly modified, replacing the oil diffusion pump with a mercury diffusion pump and the water-cooled baffle with a Freon −22 refrigerated baffle, in order to reduce the instrument background levels. Mass spectra were visualized in real time on an oscilloscope. With this early instrument, spectra were collected at the rate of 2000 scans/s, scanning the range m/z 1–6000.

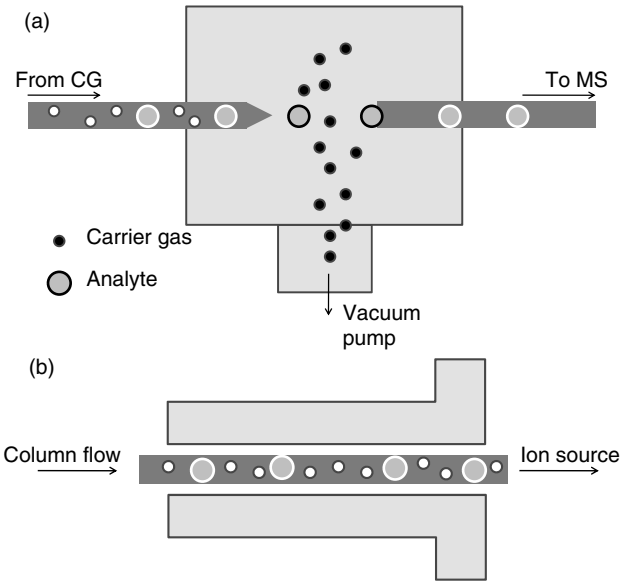

FIGURE 1.11 Coupling of GC to mass spectrometers via (a) a jet separator or (b) direct introduction (reprinted from Ref. 112, with permission of John Wiley & Sons, Inc.).

Initial problems in coupling the two techniques arose, in part, from the use of packed columns in GC. In such columns, flow rates are in the order of 10–20 mL/min, which are not compatible with the MS vacuum system [110]. Hence, ways to reduce the flow rate from the GC column before entering the mass spectrometer were needed. A number of different interfaces were developed to alleviate this problem, but only the more commonly employed ones are discussed here.

In molecular (or jet) separators (Figure 1.11a), introduced by Ryhage in 1964, the effluent from the GC feeds into an evacuated chamber through a restricted capillary [111]. An expanding, supersonic jet, composed of carrier gas and sample molecules, is formed at the tip. Lower-molecular-weight compounds diverge from the jet and are lost, mainly as a result of collisions. The higher-molecular-weight compounds form the core of the jet that is subsequently sampled into the mass spectrometer [112]. Not only is flow rate reduced, but sample components are enriched prior to entering the mass spectrometer. However, transport efficiency is low ($\sim 40\%$), and the separator discriminates against lower-molecular-weight sample components [112].

An alternative to molecular separators is the open-split interface that splits the flow, thereby reducing the total gas flow entering the mass spectrometer. The interface uses a T-connector that contains a restrictor tube [113,114]. The GC column feeds into one end of the restrictor, and a second length of fused silica feeds from the restrictor into the mass spectrometer. The length and diameter of this second piece of fused silica is chosen such that a compatible flow rate is delivered to the mass spectrometer. A flow of helium into the T-connector removes excess carrier gas flow, and the connector is

heated to prevent condensation of the separated components [113]. Although no sample enrichment is possible, this interface allows switching of columns without the need to vent the mass spectrometer. Additionally, the interface is compatible with a wide range of GC flow rates. However, transport efficiency into the mass spectrometer was low (20–50%), which can have a detrimental effect on the sensitivity achievable [113,115].

In modern GC-MS instruments, the need for molecular separators or flow splitting is eliminated with the use of wall-coated open tubular (capillary) columns. Flow rates for these columns are generally less than 2 mL/min, which is more compatible with the vacuum system of the mass spectrometer [113]. As a result, the GC column can be fed directly into the ion source, via a heated transfer line, with no restrictions necessary (Figure 1.11b). As with the open-split interface, there is no sample enrichment, but this is not necessary as there is 100% transport efficiency from the column into the ion source. Despite the simplicity of this approach, there are some disadvantages. Since all the effluent directly enters the ion source, there is an increased risk of contamination and, since the end of the column is under high vacuum, the mass spectrometer must be vented in order to change the column [110]. Nonetheless, the vast majority of GC-MS applications today use this direct coupling interface.

Considering commercial GC-MS instruments, numerous ionization and mass analyzer combinations are available. Most commonly, EI, positive CI, and negative CI are offered, with one manufacturer offering a pulsed positive ion–pulsed negative ion (PPIPNI) CI source. The single quadrupole, triple quadrupole, and ion trap (linear or quadrupole) are among the more common mass analyzers used in benchtop GC-MS instruments. However, hyphenated instruments using time-of-flight mass analyzers and magnetic sector analyzers are readily available commercially.

1.5.2 Liquid Chromatography–Mass Spectrometry

Liquid chromatography (LC) is often used to analyze samples that are not amenable to GC analysis, namely, nonvolatile or thermally labile compounds. As it is beyond the scope of this section to discuss LC theory and principles, interested readers are directed to many of the excellent texts available [113,116]. In the early 1970s, research efforts began to focus on coupling LC with MS. As stated previously, MS offers definitive identification of samples, and is a highly sensitive detector. Additionally, an LC-MS system allows separation and detection of samples that are not readily analyzed by GC.

However, interfacing LC with MS proved more difficult than for GC, for a number of reasons. Flow rates in LC are in the range 0.1–10 mL/min, although more typically 1–2 mL/min for conventional LC [112,113]. Considering methanol as an example, a liquid flow rate of 1 mL/min corresponds to a gas flow rate of 593 mL/min at atmospheric pressure [112], which is too high to be introduced directly into the mass spectrometer. Furthermore, the mobile-phase composition is seldom compatible with MS because of the presence of various nonvolatile additives. Since the late 1970s, a number of different interfaces have been developed and commercialized [117]. These interfaces are based mainly on (1) removing the liquid mobile

phase from the effluent, (2) splitting the effluent flow, or (3) ionizing the effluent at atmospheric pressure, prior to entering the mass spectrometer. This section is intended as only a very brief overview of the more common interfaces that were developed and those that are in current use; interfaces and their development are discussed in greater detail in the literature, and readers are directed to these resources for further details [112,116].

The moving-belt interface developed by McFadden et al. was the first interface to be commercialized in 1977 [117,118]. The interface was based on an earlier design by Scott et al. and involved removing the mobile phase prior to entering the mass spectrometer [119]. The column effluent was deposited on a ribbon composed of stainless steel or polyimide that was continuously moving. The ribbon passed under heaters and through vacuum locks to evaporate the mobile-phase solvent. The belt entered the mass spectrometer and the remaining sample residue was vaporized via a flash vaporizer directly attached to the ion source. Because of the speed and efficiency of vaporization, the sample entered the ion source with little decomposition and was subsequently ionized by EI or CI. On leaving the ion source, the belt passed over another heater to clean off any remaining residues and minimize carryover into the next sample. On the basis of this design, sample components had to be volatile (to some extent) to be desorbed and vaporized from the belt. Although the moving-belt interface could accommodate flow rates of 1–2 mL/min [113], obtaining reproducible spectra was dependent on depositing a uniform layer of sample on the belt. This was more difficult to achieve when water was present in the mobile phase, which gave rise to droplets, rather than a film, on the belt. In addition, the mechanical nature of the moving belt rendered it more prone to breakage and therefore, less robust [117].

Early work by Tal'roze et al. used a capillary to introduce the column effluent directly into the ion source at flow rates less than 1 μL/min [120]. Volatile analytes were subsequently ionized via EI. Baldwin and McLafferty reported the direct introduction of liquids into a CI source via a 2-mm capillary drawn into a fine tip at the end [121]. The capillary was introduced into the ion source using a normal sample probe, and the solvent was used as the reagent gas for CI. Later, a narrow capillary [75 μm i.d. (inner diameter)] was used to restrict effluent flow into the ion source [122]. However, problems occurred when the liquid evaporated in the capillary as a result of the high vacuum in the ion source. Attempts to overcome this problem by restricting the capillary had limited effectiveness as blocking of the capillary then became problematic. In 1980, Melera replaced restricted capillaries with a diaphragm that allowed the formation of a stable liquid jet [123]. Pinholes in the diaphragm restricted the effluent flow entering a desolvation chamber, where the effluent was then nebulized. As before, the mobile-phase liquid was used as the reagent gas for chemical ionization of the analytes. This design, known as the *direct liquid introduction* (DLI) *interface*, was commercialized in 1980, soon after commercialization of the moving-belt interface [117]. Niesson published a two-part review of the DLI interface, with the first part focusing on instrumental aspects and the second part on MS and applications [124,125]. The DLI interface could accommodate flow rates in the range 50–100 μL/min [112] meaning that, in order to maintain sensitivity, the interface was best used with at least microbore columns, which were not

conventionally used in routine applications. In addition, pinholes in the diaphragm were still prone to clogging [112]. With further advances in different interface designs, the DLI interface is now considered obsolete [112].

Willoughby et al. described the monodisperse aerosol generation interface for chromatography (known as "MAGIC") in 1984, which became the basis for the particle beam (PB) interface [116,126]. Aspects of interfacing LC with MS using a PB interface have been reviewed by Cappiello [127]. Similar to the moving-belt interface, the PB interface also removes the mobile phase solvent prior to ionization. The effluent is nebulized into a desolvation chamber, the outer walls of which are heated to 50–70°C [116]. The resulting droplets are dispersed, by means of a perpendicular flow of helium, and desolvated. The less volatile analyte components coagulate to form small particles, with diameters ranging from 50 to 300 nm [116]. The mixture passes through a narrow nozzle into a two-stage momentum separator. In the first stage, the pressure is typically 10 kPa. In the resulting expanding jet, the lower-mass components (mobile phase and nebulizing gas) diverge and are pumped away. The heavier mass analyte particles are sampled through a skimmer into the second pumped region (typically 30 kPa). Again, diverging particles are pumped away, leaving a beam of particles enriched in analyte that is introduced into the ion source through a transfer line. Transferred particles strike the walls of the ion source, which is heated to approximately 250°C [116]; hence, flash vaporization or disintegration of particles occurs and subsequent ionization is achieved using EI or CI. One of the main advantages of this interface is the ability to generate EI spectra from samples analyzed by LC, enabling comparison with library databases. However, the performance of the interface varies with mobile-phase composition. For example, the presence of water in the mobile phase detrimentally affects sensitivity since the high surface tension and boiling point of water prevents formation of completely solvent-free particles [127]. As such, the PB interface is now also considered obsolete [116].

Until this point in the development of LC-MS, ionization was mainly achieved by EI or CI, meaning that the analysis of nonvolatile or thermally labile sample components was limited. Although fast-atom bombardment (FAB) ionization had been reported with a moving-belt interface [112], it wasn't until the development of flow FAB interfaces in the mid 1980s [128–130] that the analysis of nonvolatile and thermally labile samples was more readily realized. In FAB, the sample is mixed with a nonvolatile matrix (typically glycerol), applied to the end of a probe, and then bombarded with a beam of fast atoms [114]. Surface atoms are ionized, and the ions are then focused and accelerated toward the mass analyzer [114]. Thus, in developing the FAB interface, the additional concern of adding the matrix to the sample had to be addressed. Technological advances in the development of the flow–FAB interfaces, as well as applications, have been reviewed [131].

Ito et al. developed the frit FAB interface in 1985 [130] and Caprioli et al. reported the continuous-flow (Cf) FAB interface in 1986 [128]. In each case, the FAB probe is modified to accommodate a capillary through which the effluent, mixed with the FAB matrix, flows. The matrix can be mixed with the effluent pre- or postcolumn. In frit FAB, a porous stainless-steel frit is positioned at the end of the capillary, while in Cf

FAB, the capillary is directed toward a FAB target. The mobile phase evaporates at the frit or target, leaving a thin film of sample and matrix, which is then subjected to FAB [116]. In 1988, de Wit et al. introduced the coaxial CfFAB interface to enable coupling of packed microcapillary or open tubular (OT) LC columns with MS [129]. In their design, two separate capillary columns were used to deliver the column effluent and FAB matrix to the probe tip, where mixing occurred [129]. As a result, independent control of flow rates was possible [132]. Irrespective of design, typical flow rates for flow FAB interfaces are in the 5–15 μL/min range. Thus, microbore columns must be used or, if conventional packed columns are used, the effluent flow must be split, which affects sensitivity [116].

The development and commercialization of atmospheric-pressure ionization (API) sources in the mid- to late 1980s widened the range of sample types that could be analyzed by LC-MS [117]. In fact, many of the previously discussed interfaces are obsolete, with commercial LC-MS systems using API sources as interfaces. In these sources, the effluent is ionized at atmospheric pressure and the resulting ions are continuously sampled into the mass spectrometer for separation and detection. Today, two API sources dominate in commercially available LC-MS instruments: electrospray ionization (ESI) and atmospheric-pressure chemical ionization (APCI). These sources have been discussed elsewhere in this chapter and thus are not described again here. Examples of interfaces for ESI- and APCI-LC-MS are given in Figures 1.12 and 1.13, respectively.

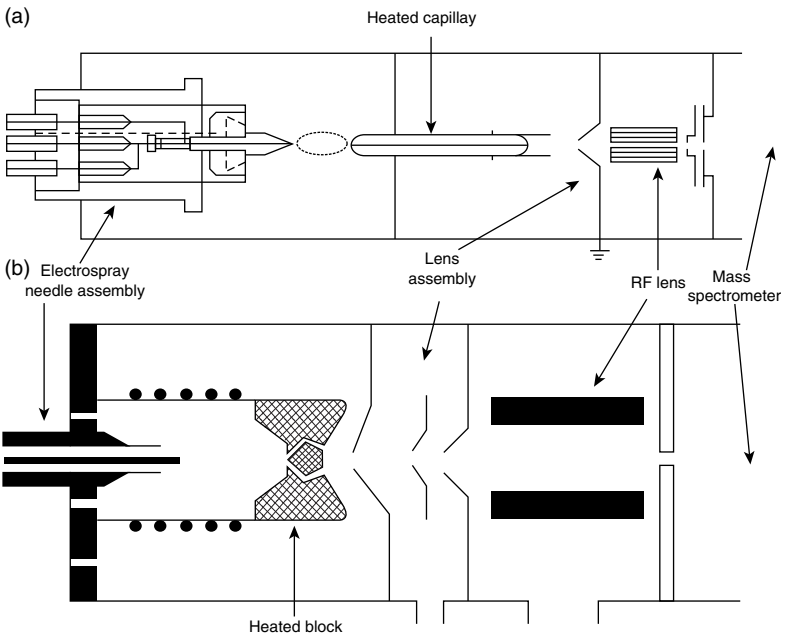

FIGURE 1.12 Interfaces for electrospray LC-MS: (a) heated capillary and (b) heated block designs (reprinted from Ref. 117, with permission of John Wiley & Sons, Inc.).

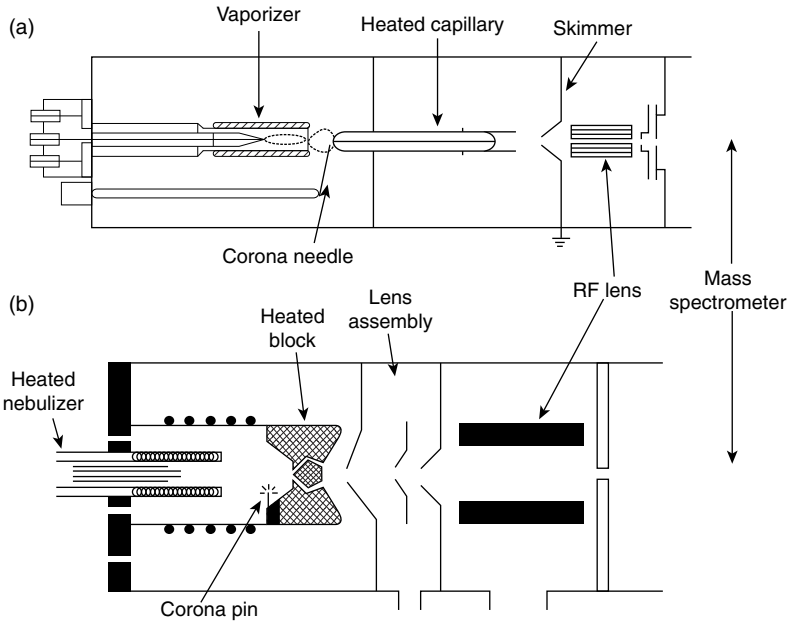

FIGURE 1.13 Interfaces for atmospheric-pressure chemical ionization LC-MS: (a) Thermofinnigan, Hemel Hempstead, UK; (b) Micromass UK Ltd., Manchester, UK (reprinted from Ref. 117, with permission of Wiley & Sons, Inc.).

Research in the late 1960s and early 1970s by Dole and coworkers [133–135] introduced the concept of electrospray, in which molecular beams of macromolecules were generated in vacuo. In 1984, Yamashita and Fenn applied this concept to create molecular beams of analytes sufficiently small to be mass analyzed using a conventional quadrupole analyzer [136]. Later work by Fenn's group described the use of the electrospray source as an interface in LC-MS [137]. It was with these developments in ESI that attention returned to investigating the use of APCI as an interface in LC-MS, even though the concept of APCI was first reported in the literature in the early 1970s [138].

Atmospheric-pressure chemical ionization is used for the ionization of low- to medium-polarity compounds while higher-molecular-weight, polar compounds are ionized by ESI. In terms of ionization, APCI typically generates singly charged ions of the molecular species, with little fragmentation. Electrospray ionization is also considered a mild ionization process but, in contrast to APCI, large molecules with numerous ionizable sites will form multiply charged ions. This not only increase sensitivity but also enables the analysis of compounds with molecular weights beyond the working mass range of the spectrometer [114].

For APCI, flow rates range from 100–200 μL/min to 1–2 mL/min, while for ESI, flow rates range from 1 μL/min to 1 mL/min [139]. Further modifications have resulted in ESI sources that operate at significantly lower flow rates. Emmett and Caprioli described a micro-ESI source that accommodated flow rates in the range

300–800 nL/min [140], while Wilm and Mann described the nano-ESI, which used flow rates as low as 20 nL/min [141]. Lower flow rates are not detrimental to sensitivity, which, in ESI, is dependent on concentration rather than sample volume introduced. In fact, lower flow rates can be advantageous in certain applications owing to less sample consumption.

In certain applications, such as the identification of potential drug candidates in the pharmaceutical industry, it is often desirable to use a combination of ionization techniques for full analyte characterization. This impetus was the driving force behind the development of combined ESI-APCI sources. Gallagher et al. reported a combined source for high-throughput LC-MS analyses [142]. Within a single analysis, ESI and APCI scans were alternately collected with polarity switching. Nowadays, several instrument manufacturers offer dual-source LC-MS instruments, allowing sample characterization using two different ionization techniques while eliminating the need to change and re-optimize hardware.

In terms of commercial LC-MS instruments, ESI and APCI sources are the most commonly available, and many manufacturers also offer a combined ESI/APCI source. Each manufacturer also offers a range of LC-MS instruments, incorporating different mass analyzers. Single-quadrupole, ion trap, triple-quadrupole, and time-of-flight (TOF) analyzers are most common, although quadrupole-TOF (Q-TOF) and Fourier transform ion cyclotron resonance (FT-ICR) analyzers are also available.

1.5.3 Capillary Electrophoresis–Mass Spectrometry

Originating with the initial work of Jorgenson and Lukacs, capillary electrophoresis (CE) has evolved to become a sensitive and efficient separation technique [143,144]. Samples are carried through a narrowbore fused-silica capillary (10–100 cm long, 25–100 μm i.d.) in a flow of buffer, and are separated under the influence of an applied electric field [113]. Separated components can be detected inline using optical detectors (e.g., UV absorbance or fluorescence) to generate an electropherogram, which is a plot of detector response versus migration time. In CE, separation of charged and uncharged species in a single analysis is possible, and today, the term *capillary electrophoresis* is applied to a range of different separation modes, all based on the same principles, but chosen according to sample type. For example, in capillary zone electrophoresis (CZE), initially described by Jorgenson and Lukacs [143,144], separation is based on differences in hydrodynamic radius/charge ratios [145]. In capillary gel electrophoresis, a molecular sieve is used to separate samples according to size, while in capillary isoelectric focusing, amphoteric samples are separated based on differences in isoelectric points [113]. Several texts and articles are available that discuss the history, development, and applications of capillary electrophoresis [113,146–150].

Because of the relatively short, narrowbore capillary columns used, flow rates in CE are in the nanoliter range, meaning that coupling to MS is more amenable than is coupling LC. Additionally, due to the low flow rates, highly sensitive detectors are desirable. This led research efforts to focus on coupling CE with MS with

Olivares et al. first reporting online MS detection for CZE in 1987 [151]. Similar to chromatographic techniques, using MS as a detector offers definitive identification of sample components, as well as the desired sensitivity. More recently, a number of review articles have been published that discuss the development of interfaces that have enabled coupling of CE with MS [145,152,153]. Hence, this section focuses only on the common interface that uses an electrospray ionization source to couple the two instruments.

Using an ESI source, interface configurations can be subdivided into two classes: sheath flow interfaces and sheathless interfaces [152]. In the former, the voltage necessary for ESI is applied to the CE buffer indirectly by means of a sheath liquid while in the latter, the voltage is applied directly to the buffer. With sheath flow interfaces, the buffer composition can be altered to be more compatible with subsequent analysis and detection techniques (i.e., ESI and MS); however, with the addition of the sheath liquid, the buffer and hence, sample components, are diluted, which can have detrimental effects on sensitivity. The sheathless interface configuration can, therefore, offer greater sensitivity since there is no dilution effect, but it is more limited in the choice of compatible CE buffers.

Considering the sheath flow interface (Figure 1.14), two configurations are common: the coaxial sheath flow and the liquid junction configurations. In the coaxial configuration, the CE capillary is surrounded by a wider-diameter, outer tube. The sheath liquid is introduced, either hydrodynamically or by external

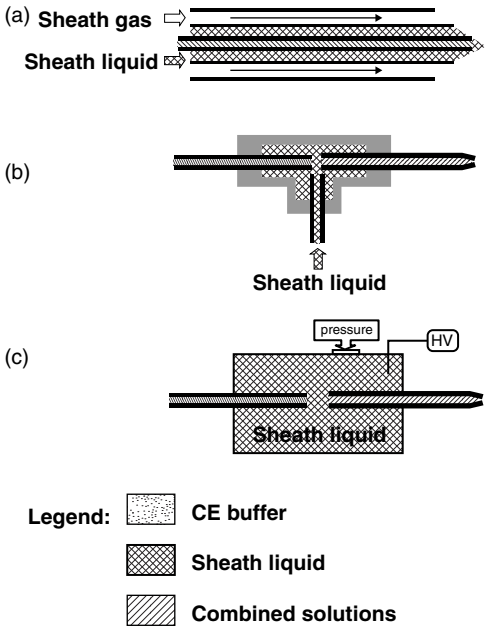

FIGURE 1.14 Sheath flow interfaces for CE-MS: (a) coaxial sheath flow with sheath gas; (b) liquid junction; (c) pressurized liquid junction (reprinted from Ref. 195, with permission of Elsevier).

pumping, and flows through this tube. The CE buffer and sheath liquid mix at the Taylor cone, at the tip of the electrospray emitter. Since mixing only occurs as the separated components leave the capillary, the separation process is undisturbed. A further modification to this configuration involves the addition of a second outer tube that encompasses the previous assembly. This tube accommodates a flow of sheath gas, which may be necessary to stabilize the spray and facilitate droplet formation, particularly at higher flow rates [152,153].

The liquid junction configuration is similar in principle, except for the position at which the buffer and sheath liquid are mixed. The end of the capillary and ESI emitter are housed in a T-junction, with a narrow gap (typically 20–50 μm) between the two [152]. The sheath liquid is introduced orthogonally into the gap. There is less dilution in this configuration such that sensitivity is not as detrimentally affected as in the coaxial configuration. However, with the orthogonal introduction of liquid, band broadening can occur as the separated components leave the capillary, which can lead to poorer resolution. This effect can be overcome using the pressurized liquid junction configuration that was described by Fanali [154]. In essence similar to the liquid junction, the main differences are the larger gap between the capillary and ESI emitter (100 μm) and the fact that the junction is contained within a pressurized reservoir of sheath liquid [152,154]. With the applied pressure, band broadening is minimized, leading to improved resolution and separation efficiency [152]. In addition, although the CE buffer is still diluted with sheath liquid, the dilution factor is not as great as with the coaxial and unpressurized liquid junction configurations [152].

Since no sheath liquid is present in sheathless interfaces, the necessary voltage must be applied directly to the CE buffer, which can be achieved in a number of ways (Figure 1.15). In the first report of CE with online MS detection, Olivares et al. terminated the CE capillary in a stainless-steel sheath [151]. A potential was applied

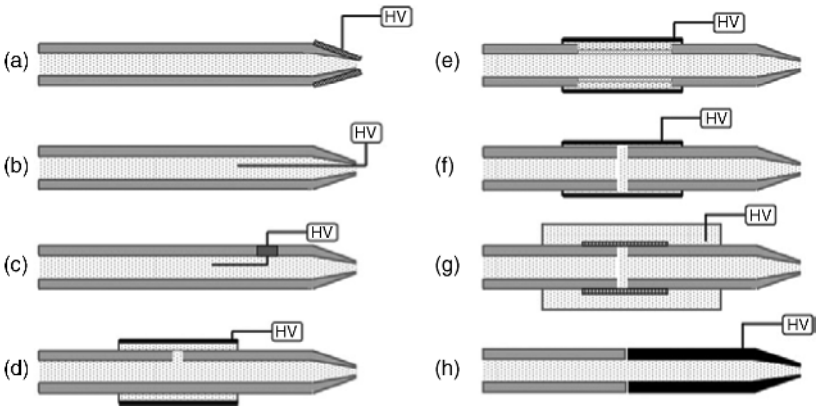

FIGURE 1.15 Sheathless interfaces for CE-MS, illustrating methods used to create electrical contact: (a) conductive coating applied to emitter tip; (b) wire inserted at tip; (c) wire inserted through hole; (d) split-flow interface with metal sheath; (e) porous, etched capillary walls in metal sleeve; (f) junction with metal sleeve; (g) microdialysis junction; (h) junction with conductive emitter tip (reprinted from Ref. 195, with permission of Elsevier).

to the sheath, which was used as the CZE cathode, as well as the electrospray needle. In later work, silver vapor was deposited onto the capillary and ESI needle to improve the electrical contact [155]. Other options for sheathless interfaces include coating the capillary end with a metal [153]. The sprayer tip can also be metal-coated or fabricated from a conductive material (e.g., metal or polymer), with the capillary end positioned in direct contact with the tip [153]. Alternatively, a wire electrode can be inserted into the capillary, either through the end of the capillary or via a small hole drilled near the end of the capillary [152,153].

While ESI sources constitute the most common interfaces for CE-MS, the use of other ionization sources as interfaces has been reported, which can widen the range of sample types that can be separated and detected by CE-MS. Inductively coupled plasma (ICP) sources are widely used as interfaces for applications involving elemental speciation and the development, and applications of CE-ICP-MS were reviewed by Kannamkumarath et al. in 2002, by Michalke in 2005, and by Álvarez-Llamas et al., also in 2005 [156–158].

Tanaka et al. reported an APCI interface for CE-MS [159]. A commercial APCI manifold was modified to incorporate a stainless–steel tube that surrounded the CE capillary and accommodated a coaxial flow of sheath liquid. A nebulizing gas was also introduced. The steel tube, containing the capillary, was then positioned in the APCI nozzle for subsequent ionization of the sample [159]. As mentioned in Section 1.5.1, APCI offers ionization of less-polar compounds that are not amenable to ESI. In addition, CE–atmospheric-pressure photoionization–MS (CE-APPI-MS) has been reported in the literature, by modifying an APPI source originally intended for LC-MS [160]. A wider range of CE buffers can be used with APPI sources; nonvolatile buffers did not cause the analyte signal suppression observed using ESI [160].

In a review of CE-MS developments and applications, Schmitt-Koplin and Englmann reported on trends in mass analyzers used in the hyphenated instruments [161]. Between 1987 and 2001, the majority of CE-MS publications described the use of single-quadrupole or triple-quadrupole mass analyzers. Tandem quadrupole, ion trap, time-of-flight (TOF), Fourier transform ion cyclotron resonance (FT-ICR), and sector field analyzers were also reported, albeit in fewer publications. With the exception of the tandem quadrupole, publications using each type of mass analyzer increased between 2001 and 2004. The greatest increase was observed for the ion trap, followed by the single quadrupole, then triple quadrupole, and TOF. By 2004, less than 10 publications reported the use of either FT-ICR or sector field analyzers [161].

1.5.4 Ion Mobility Spectrometry–Mass Spectrometry

Ion mobility spectrometry (IMS) separates ions on the basis of differences in differential mobility through a weak, uniform electric field, in the presence of a counterflow of drift gas [162,163]. Mobility depends on collision cross section and thus, ions are separated according to size-to-charge ratio [164]. The technique was initially termed *plasma chromatography* and in fact, one of the first papers on IMS

described a hyphenated GC-IMS-MS instrument [165]. Samples were separated by GC, detected by IMS or further separated on the basis of mobility, then mass-separated and detected by MS. A ^{63}Ni source was initially used as the ion source, limiting IMS to the analysis of volatile samples in the vapor phase [163]. However, today, atmospheric-pressure ionization sources such as ESI and MALDI are also used, thus increasing the range of sample types amenable to analysis by IMS [163]. For further details on the history, theory, and principles of IMS, readers are directed to the excellent text by Eiceman and Karpas that covers these aspects in detail [162].

Coupling IMS with MS is advantageous because of differences in separation mode between the two techniques. In IMS, ions are separated according to size-to-charge ratio while in MS, separation is based on mass-to-charge ratio. Hence, isomers and conformers can be separated by IMS, which is not possible by MS. However, definitive identification of analytes is possible by MS but not by IMS alone since collision cross section is not sufficiently specific. In the following section, interface designs and IMS/MS instrument configurations are discussed; however, this discussion is certainly not exhaustive, and readers are directed to several review articles and texts that are available in the literature for further details [162–164].

In coupling IMS and MS, differences in operating pressures have to be considered as well as differences in electrical potentials of the two instruments and the interface. Two interface designs are commonly employed. In the first, a pinhole orifice (20–50 μm), or skimmer cone with orifice diameter 100 μm, is used and ions are transferred directly from the IMS drift tube to the high vacuum of the mass spectrometer [162]. The second design uses two skimmer cones, or one skimmer cone and a large pinhole membrane, to transfer ions from the drift tube through two differentially pumped regions, into the mass spectrometer [162]. To ensure that ions can pass from the drift tube, through the interface, and into the mass spectrometer, it is necessary to increase the potential of the interface with respect to the mass analyzer (particularly for quadrupoles) and increase the potential of the drift tube with respect to the interface. A series of ion lenses are also incorporated into the interface to focus the ion beam into the mass spectrometer.

One of the early commercially available IMS/MS instruments, the Alpha II PC/MS, incorporated a quadrupole mass analyzer and the drift tube contained two ion gates to enable different modes of data acquisition (Figure 1.16) [164]. The entrance gate was positioned at the beginning of the drift tube, allowing ions to enter, while the exit gate was positioned at the end of the tube, allowing ions to leave the drift tube and enter the mass spectrometer. With both gates open, ions in the drift tube continually entered the mass analyzer, which was scanned to generate a mass spectrum of all ions in the sample. By pulsing the entrance gate and keeping the exit gate open, ions entered the drift tube (similar to operation in standalone IMS systems) and passed into the mass analyzer, which was operated in total-ion monitoring mode, enabling all ions to be detected, albeit with no mass separation. By gating both gates with suitable delays, ions of a selected mobility entered the mass analyzer, which was tuned to a specific m/z for ion identification. Throughout the 1970s and 1980s, most of the research conducted used instruments similar to the aforementioned design, and MS was essentially seen as a selective detector for the ion mobility spectrometer [164].

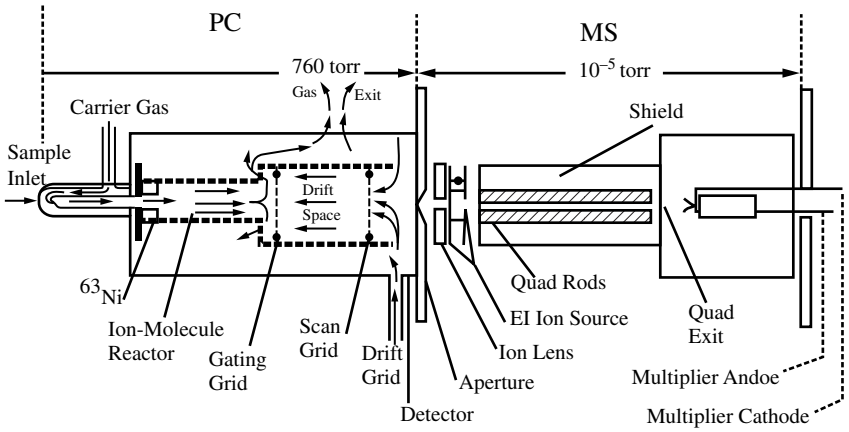

FIGURE 1.16 Alpha II plasma chromatography/mass spectrometry interface (reprinted from Ref. 196, with permission of Elsevier).

A later IMS–quadrupole MS instrument, manufactured by PCP Inc., included an EI source in the mass spectrometer, thus allowing ionization of neutral molecules that entered from the drift tube [162]. Dwivedi et al. reported the use of an IMS–quadrupole MS system for chiral separation of pharmaceuticals, carbohydrates, and amino acids that was achieved through addition of a chiral additive to the drift gas [166]. Subsequent separation in the drift tube was based not only on size and charge but also on stereospecific interactions with the chiral gas. Further details and applications of IMS–quadrupole MS have been reviewed and are available in the literature [162,163].

Into the 1990s, developments in instrument design continued to generate and sustain interest in IMS/MS. Guevremont et al. modified a commercially available IMS/MS instrument, replacing the ^{63}Ni source with an ESI source and replacing the quadrupole with a time-of-flight mass analyzer [167]. After passing through an orifice interface (25 μm diameter) between the drift tube and mass spectrometer, ions passed through a series of four lenses and were accelerated into the flight region by application of simultaneous pulses to two grids (Figure 1.17). In terms of data acquisition, it was possible to "gate" individual IMS peaks; that is, data were acquired only when an IMS peak of interest entered the mass analyzer [167].

In TOF-MS, spectra are collected in the microsecond range, while ion mobility spectra are collected in the millisecond range. This means that, when the two are coupled, hundreds of mass spectra can be collected for each ion in the ion mobility spectrum [163]. The advantages of this aspect were highlighted by Clemmer and coworkers for the gas-phase separation of protease digests [168]. As the mass analyzer continuously scanned throughout the duration of the ion mobility cycle, the sample could be characterized in terms of ion mobility, m/z, and intensity. More recently, IMS-TOF-MS has been used further in the separation of protein–peptide mixtures [169,170], and amphetamine-type drugs [171], as well as for the characterization of oligosaccharides [172], among other applications [163].

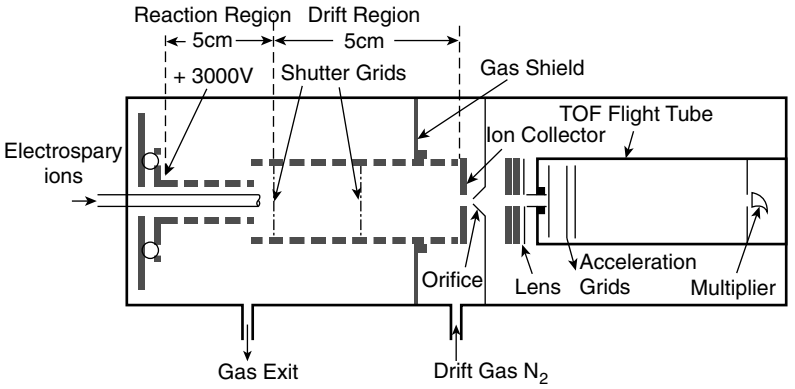

FIGURE 1.17 Coupling of ion mobility spectrometry with time-of-flight mass spectrometry (reprinted from Ref. 167, with permission of the American Chemical Society).

Clowers and Hill described coupling IMS with a quadrupole ion trap (QIT) MS [173]. The drift tube contained two Bradbury–Nielson gates. Opening of the second gate was delayed with respect to the first to allow ions of a specific mobility to enter the trap. The process was repeated to accumulate sufficient population of the specific mobility ion in the trap for MS^n experiments [173]. A quadrupole ion trap was also used by Creaser et al. in their tandem ion trap/ion mobility spectrometer [174]. In this design, the ion trap could be used in the conventional sense as a mass analyzer or alternatively, as an ion source for IMS.

Although not as common as the mass analyzers discussed above, IMS has been coupled with Fourier transform ion cyclotron resonance mass spectrometers [163]. Tang et al. incorporated a two-gate system and coupled the two instruments via a flared inlet capillary interface [175]. Thus, separation occurred in the ion mobility spectrometer and ions of specific mobility were selected for subsequent mass analysis. Using this system, separation of two peptides, as well as separation of two isomeric phosphopeptides, was demonstrated [175].

1.6 PROSPECTS FOR MASS SPECTROMETRY

Mass spectrometry is indeed a powerful tool for chemical analysis that has been widely applied in a variety of areas related to scientific research, industrial production, and governmental regulations. An even wider range of applications of MS can be foreseen for applications such as production quality control, food safety regulation, disease diagnosis or personal healthcare, and security — applications that are highly dependent on the availability of MS analysis systems with acceptable size and cost and a minimum requirement of skills for operation. After over a century of development, the mass spectrometers themselves, as in-laboratory instruments, have become more and more automated and robust, although the cost of ownership and maintenance is still far beyond what is acceptable for use at pharmacies, grocery

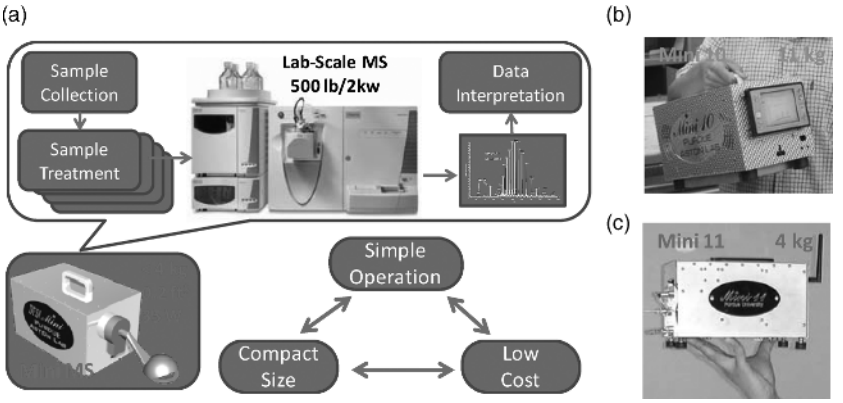

FIGURE 1.18 (a) Conceptual schematic of a miniaturized mass spectrometry analytical system; (b) Mini 10 and (c) Mini 11 handheld ion trap mass spectrometers (illustrations reprinted from Ref. 176, with permission from *Annual Reviews*).

stores, or households. Current mass spectrometric chemical analysis procedures are also highly dependent on sample type, which ultimately requires the personnel performing the analysis to have the knowledge and experience for the sample preparation and data interpretation. These are the limiting factors that prevent the current MS analysis systems to be employed outside of analytical laboratories. Since the 1990s, some major efforts have been put into the development of miniature mass spectrometers of all types [176] (see Figure 1.18). Handheld mass spectrometers weighing only 5 kg have been developed with the capability of coupling in vacuo as well as atmospheric-pressure ionization sources [177,178]. A discontinuous atmospheric-pressure interface (DAPI) [179] was developed, which opens periodically for ion introduction. It allowed the transfer of ions generated in air, such as by ESI or APCI, into the vacuum manifold for mass analysis without using complicated differential pumping stages or high-capacity pumping systems. The capabilities of these small instruments have been demonstrated with the analysis of volatile organic compounds (VOCs) in air and water as well as nonvolatile compounds, including peptides and proteins in samples in condensed phases. Such miniature instrumentation represents the state of the art in MS technologies, exemplifying how MS systems can be developed with much smaller size, lower weight, and lower cost, which ultimately economically justifies the development of specialized MS systems targeting narrow ranges of applications.

With the emerging possibilities of miniature mass spectrometers, finding solutions for simplifying the sample preparation is becoming highly desirable. Ambient ionization methods, which aim at the direct sampling of analytes from complex sample matrices, have been developed and applied for MS analysis with minimal or no sample pre-treatment. Starting with desorption electrospray ionization (DESI) [180] and direct analysis in real time (DART) [181], more than 20 ambient ionization methods [182–184] have been developed since 2004. The majority of these methods use charged droplets, lasers, or plasma to desorb and ionize the

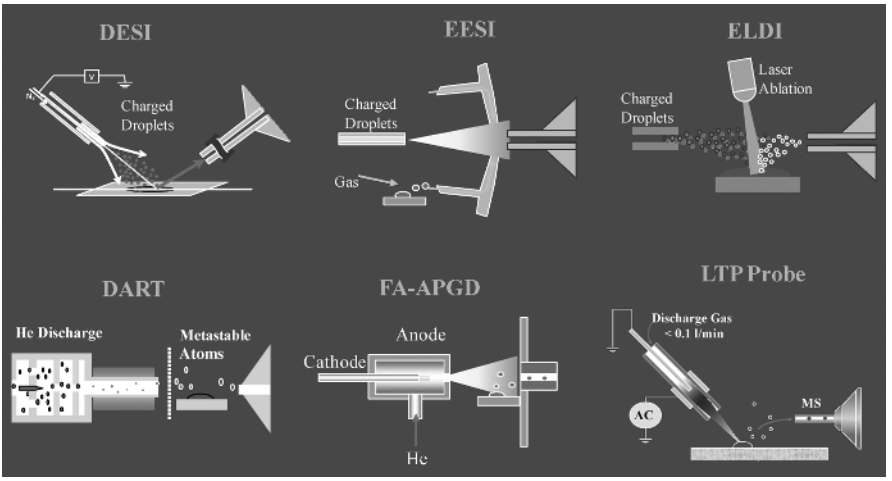

FIGURE 1.19 Some ambient ionization methods. DESI = desorption electrospray ionization [180]; EESI = extractive electrospray ionization [197,198]; ELDI = electrospray-assisted laser desorption/ionization [199]; DART = direct analysis in real time, FA-APGD = flow afterglow atmospheric-pressure glow discharge [200]; LTP = low-temperature plasma [183].

analytes from samples in condensed phases. The processes of desorption and ionization can be simultaneous or sequential (Figure 1.19), depending on the individual methods, but all techniques generally require little time for gas-phase ions to be generated for MS analysis. The direct analysis of complex samples has been demonstrated using these methods, including the analysis of nonvolatile organics, such as explosives, from various surfaces [185], steroids and metabolites in urine [186,187], ingredients in drug tablets [188], fatty acids from olive oil [189], and lipids from raw tissue [190]. MS imaging of raw tissues has also been developed with DESI for lipid [191] and drug distributions [192]. Most of the ambient ionization methods are implemented for qualitative or semiquantitative analysis, since sample treatments, including the addition of internal standards, are minimized to simplify the procedure. A new method of generating ions directly from paper loaded with samples was developed by applying a high voltage to the paper wetted with solution; this method of analysis has been applied for therapeutic drug monitoring with direct analysis of dried blood spots (DBS) and highly quantitative information can be obtained over the therapeutic ranges of various drugs, including imatinib (Gleevec) and atenolol [193].

The combination of ambient ionization methods and miniature mass spectrometers potentially will provide a unique instrumentation platform for the development of MS analysis systems of small size, low cost, more importantly, with simplified analysis procedures. It is foreseen that a wide variety of miniature MS systems, each targeting specialized applications, will be developed to allow personnel inexperienced in analytical chemistry to be able to use them outside analytical laboratories. Knowledge

and experience accumulated in chromatography, reactive ionization, and selective derivatization in real time will be used in the development of sampling devices that have enhanced specificity and sensitivity for target analytes in complex samples. The first adoption of such miniature MS systems will likely occur with applications in areas such as clinical diagnosis or therapy, where the need for complex mixture analysis by MS has been demonstrated and simple analysis procedures are mandated by governmental regulations.

REFERENCES

1. Cooks, R. G.; Ouyang, Z. (2002), The American Society for Mass Spectrometry and Allied Topics, Orlando, FL.
2. Aston, F. W. (1922), Nobel Prize acceptance speech, Stockholm, Sweden.
3. Parkins, W. E. (2005), *Phys. Today 58*, 45–51.
4. Palmer, P. T.; Limero, T. F. (2001), *J. Am. Soc. Mass Spectrom. 12*, 656–675.
5. Nemes, P.; Vertes, A. (2007), *Anal. Chem. 79*, 8098–8106.
6. Nie, Z.; Cui, F.; Tzeng, Y. K.; Chang, H. C.; Chu, M.; Lin, H. C.; Chen, C. H.; Lin, H. H.; Yu, A. L. (2007), *Anal. Chem. 79*, 7401–7407.
7. Dalton, J. (1808), *A New System of Chemical Philosophy*; Henderson & Spalding; London.
8. Prout, W. (1815), *Ann. Philos. 6*, 321–330.
9. Prout, W. (1816), *Ann. Philos. 7*, 111–113.
10. Griffiths, I. W. (1997), *Rapid Commun. Mass Spectrom. 11*, 3–16.
11. Thomson, J. J. (1897), *Philos. Mag. 5*, 293–316.
12. `http://nobelprize.org`; (2009).
13. Grayson, M.; Brenna, J. T.; Busch, K. L.; Caprioli, R. M.; Cotter, R. J.; Grigsby, R. D.; Judson, C. M.; Ramanathan, R.; Siuzdak, G.; Story, M. S.; Thomas, J. J.; WIlloughby, R. C.; Yergey, A. L. (2002), *Measuring Mass: From Positive Rays to Protein*, American Society for Mass Spectrometry, Santa Fe, NM.
14. Thomson, J. J. (1913), *Proc. Roy. Soc. Lond. A (Containing Papers of a Mathematical and Physical Character) 89*, 1.
15. Downard, K. M. (2007), *Mass Spectrom. Rev. 26*, 713–723.
16. Aston, F. W. (1920), *Nature 105*, 617–619.
17. Budzikiewicz, H.; Grigsby, R. D. (2006), *Mass Spectrom. Rev. 25*, 146–157.
18. De Laeter, J. R. (2009), *Mass Spectrom. Rev. 28*, 2–19.
19. Nier, A. O. (1989), *J. Chem. Educ. 66*, 385–388.
20. Cooks, R. G.; Beynon, J. H.; Caprioli, R. M.; Lester, G. R. (1973), *Metastable Ions*, Elsevier, Amsterdam.
21. McLafferty, F. W. (1959), *Anal. Chem. 31*, 82–87.
22. McLafferty, F. W. (1966), *Interpretation of Mass Spectra*, Benjamin.
23. McLafferty, F. W.; Turucek, F. (1993), *Interpretation of Mass Spectra*, 4th ed., University Science Books, Sausalito, CA.

24. Busch, K. L.; Glish, G. L.; McLuckey, S. A. (1988), *Mass Spectrometry/Mass Spectrometry: Techniques and Applications of Tandem Mass Spectrometry*; VCH Publishers, New York.
25. Gohlke, R. S.; McLafferty, F. W. (1993), *J. Am. Soc. Mass Spectrom. 4*, 367.
26. Bouchoux, G. (2007), *Mass Spectrom. Rev. 26*, 775–835.
27. Biemann, K.; Oro, J.; Toulmin, P.; Orgel, L. E.; Nier, A. O.; Anderson, D. M.; Simmonds, P. G.; Flory, D.; Diaz, A. V.; Rushneck, D. R.; Biller, J. A. (1976), *Science 194*, 72–76.
28. Biemann, K.; Gapp, F.; Seibl, J. (1959), *J. Am. Chem. Soc. 81*, 2274–2275.
29. Sundqvist, B.; Macfarlane, R. D. (1985), *Mass Spectrom. Rev. 4*, 421–460.
30. Gelpi, E. (2009), *J. Mass Spectrom. 44*, 1137–1161.
31. Fenn, J. B.; Mann, M.; Meng, C. K.; Wong, S. F.; Whitehouse, C. M. (1989), *Science 246*, 64–71.
32. Karas, M.; Bachmann, D.; Bahr, U.; Hillenkamp, F. (1987), *Int. J. Mass Spectrom. Ion Process. 78*, 53–68.
33. Tanaka, K.; Waki, H.; Ido, Y.; Akita, S.; Yoshida, Y.; Matsuo, T. (1988), *Rapid Commun. Mass Spectrom. 2*, 151–153.
34. Yates, J. R. (1998), *J. Mass Spectrom. 33*, 1–19.
35. Asara, J. M.; Schweitzer, M. H.; Freimark, L. M.; Phillips, M.; Cantley, L. C. (2007), *Science 316*, 280–285.
36. Franck, J.; Arafah, K.; Elayed, M.; Bonnel, D.; Vergara, D.; Jacquet, A.; Vinatier, D.; Wisztorski, M.; Day, R.; Fournier, I.; Salzet, M. (2009), *Molec. Cell. Proteom. 8*, 2023–2033.
37. Zubarev, R. A.; Kelleher, N. L.; McLafferty, F. W. (1998), *J. Am. Chem. Soc. 120*, 3265–3266.
38. Syka, J. E. P.; Coon, J. J.; Schroeder, M. J.; Shabanowitz, J.; Hunt, D. F. (2004), *Proc. Nat. Acad. Sci. 101*, 9528–9533.
39. Gross, M. L.; Caprioli, R. M., eds. (2007), *The Encyclopedia of Mass Spectrometry*, Vol. 6, *Ionization methods*, Elsevier, Burlington, MA.
40. McLafferty, F. W. (1980), *Acct. Chem. Res. 13*, 33–39.
41. de Hoffmann, E.; Stroobant, V. (2001), *Mass Spectrometry: Principles and Applications*, 2nd ed., Wiley, New York.
42. Downard, K. (2004), *Mass Spectrometry: A Foundation Course*, Royal Society of Chemistry, Cambridge, U.K.
43. Watson, J. T.; Sparkman, O. D. (2004), *Introduction to Mass Spectrometry: Instrumentation, Applications, and Strategies for Data Interpretation*, 4th ed., Wiley, Hoboken, NJ.
44. Burgoyne, T. W.; Hieftje, G. M. (1996), *Mass Spectrom. Rev. 15*, 241–259.
45. Paul, W.; Steinwedel, H. (1953), *Z. Naturforsch. A (Journal of Physical Sciences) 8*, 448–450.
46. March, R. E. (1997), *J. Mass Spectrom. 32*, 351–369.
47. March, R. E.; Todd, J. F. J. (2005), *Quadrupole Ion Trap Mass Spectrometry*, 2nd ed., Wiley, Hoboken, NJ.
48. Paul, W. (1990), *Rev. Modern Phys. 62*, 531–540.

49. Stafford, G. C.; Kelley, P. E.; Syka, J. E. P.; Reynolds, W. E.; Todd, J. F. J. (1984), *Int. J. Mass Spectrom. Ion Process. 60*, 85–98.
50. Ouyang, Z.; Wu, G. X.; Song, Y. S.; Li, H. Y.; Plass, W. R.; Cooks, R. G. (2004), *Anal. Chem. 76*, 4595–4605.
51. Tabert, A. M.; Goodwin, M. P.; Cooks, R. G. (2006), *J. Am. Soc. Mass Spectrom. 17*, 56–59.
52. Douglas, D. J.; Frank, A. J.; Mao, D. M. (2005), *Mass Spectrom. Rev. 24*, 1–29.
53. Cameron, A. E.; Eggers, D. F. (1948), *Rev. Sci. Instrum. 19*, 605–607.
54. Short, R. T. (1997), *Physica Scripta T71*, 46–49.
55. Cotter, R. J. (1999), *Anal. Chem. 71*, 445A–451A.
56. Guilhaus, M.; Selby, D.; Mlynski, V. (2000), *Mass Spectrom. Rev. 19*, 65–107.
57. Chernushevich, I. V.; Loboda, A. V.; Thomson, B. A. (2001), *J. Mass Spectrom. 36*, 849–865.
58. Mamyrin, B. A. (2001), *Int. J. Mass Spectrom. 206*, 251–266.
59. Ens, W.; Standing, K. G. (2005), *Biol. Mass Spectrom. 402*, 49–78.
60. Wiley , W. C.; McLaren, I. H. (1955) *Rev. Sci. Instrum. 26*, 1150–1157.
61. Colby, S. M.; King, T. B.; Reilly, J. P. (1994), *Rapid Commun. Mass Spectrom. 8*, 865–868.
62. Brown, R. S.; Lennon, J. J. (1995), *Anal. Chem. 67*, 1998–2003.
63. Koppenaal, D. W.; Barinaga, C. J.; Denton, M. B.; Sperline, R. P.; Hieftje, G. M.; Schilling, G. D.; Andrade, F. J.; Barnes, J. H. (2005). *Anal. Chem. 77*, 418A–427A.
64. Lawrence, E. O.; Edlefson, N. E. (1930), *Science 72*, 367–377.
65. Lawrence, E. O.; Livingston, M. S. (1932), *Phys. Rev. 40*, 19–35.
66. Hipple, J. A.; Sommer, H.; Thomas, H. A. (1949), *Phys. Rev. 76*, 1877–1878.
67. Sommer, H.; Thomas, H. A.; Hipple, J. A. (1951), *Phys. Rev. 82*, 697–702.
68. Wobschall, D. (1965), *Rev. Sci. Instrum. 36*, 466–475.
69. Amster, I. J. (1996), *J. Mass Spectrom. 31*, 1325–1337.
70. Marshall, A. G.; Hendrickson, C. L. (2002), *Int. J. Mass Spectrom. 215*, 59–75.
71. Comisarow, M. B.; Marshall, A. G. (1974), *Chem. Phys. Lett. 25*, 282–283.
72. Comisarow, M. B.; Marshall, A. G. (1974), *Chem. Phys. Lett. 26*, 489–490.
73. Marshall, A. G.; Hendrickson, C. L.; Jackson, G. S. (1998), *Mass Spectrom. Rev. 17*, 1–35.
74. Marshall, A. G. (2000), *Int. J. Mass Spectrom. 200*, 331–356.
75. Marshall, A. G.; Hendrickson, C. L. (2008), *Annu. Rev. Anal. Chem. 1*, 579–599.
76. Marshall, A. G.; Wang, T. C. L.; Ricca, T. L. (1985), *J. Am. Chem. Soc. 107*, 7893–7897.
77. Kingdon, K. H. (1923), *Phys. Rev. 21*, 408–418.
78. Hu, Q. Z.; Noll, R. J.; Li, H. Y.; Makarov, A.; Hardman, M.; Cooks, R. G. (2005), *J. Mass Spectrom. 40*, 430–443.
79. Perry, R. H.; Cooks, R. G.; Noll, R. J. (2008), *Mass Spectrom. Rev. 27*, 661–699.
80. Knight, R. D. (1981), *Appl. Phys. Lett. 38*, 221–223.
81. Wells, J. M.; Badman, E. R.; Cooks, R. G. (1998), *Anal. Chem. 70*, 438–444.
82. Makarov, A. (2000), *Anal. Chem. 72*, 1156–1162.
83. Scigelova, M.; Makarov, A. (2006), *Proteomics* 16–21.

84. Makarov, A.; Denisov, E.; Kholomeev, A.; Baischun, W.; Lange, O.; Strupat, K.; Horning, S. (2006), *Anal. Chem. 78*, 2113–2120.
85. Cooks, R. G.; Terwilliger, D. T.; Ast, T.; Beynon, J. H.; Keough, T. (1975), *J. Am.Chem. Soc. 97*, 1583–1585.
86. Coon, J. J.; Syka, J. E. P.; Schwartz, J. C.; Shabanowitz, J.; Hunt, D. F. (2004), *Int. J. Mass Spectrom. 236*, 33–42.
87. Brodbelt, J. S.; Wilson, J. J. (2009), *Mass Spectrom. Rev. 28*, 390–424.
88. Kalcic, C. L.; Gunaratne, T. C.; Jonest, A. D.; Dantus, M.; Reid, G. E. (2009), *J. Am. Chem. Soc. 131*, 940–942.
89. Guan, Z.; Kelleher, N. L.; O'Connor, P. B.; Aaserud, D. J.; Little, D. P.; McLafferty, F. W. (1996), *Int. J. Mass Spectrom. Ion Processes*, *157/158*, 357–364.
90. Zubarev, R. A.; Kelleher, N. L.; McLafferty, F. W. (1998), *J. Am. Chem. Soc. 120*, 3265–3266.
91. Zubarev, R. A. (2003), *Mass Spectrom. Rev. 22*, 57–77.
92. Leymarie, N.; Costello, C. E.; O'Connor, P. B. (2003), *J. Am. Chem. Soc. 125*, 8949–8958.
93. Syka, J. E. P.; Coon, J. J.; Schroeder, M. J.; Shabanowitz, J.; Hunt, D. F. (2004), *Proc. Natl. Acad. Sci. USA 101*, 9528–9533.
94. Roepstorff, P.; Fohlman, J. (1984), *Biomed. Mass Spectrom. 11*, 601–601.
95. Zubarev, R. A.; Kruger, N. A.; Fridrikkson, E. K.; Lewis, M. A.; Horn, D. M.; Carpenter, B. A.; McLafferty, F. W. (1999), *J. Am. Chem. Soc. 121*, 2857–2862.
96. Cooper, H. J.; Hakansson, K.; Marshall, A. G. (2005), *Mass Spectrom. Rev. 24*, 201–222.
97. Coon, J. J.; Syka, J. E. P.; Schwartz, J. C.; Shabanowitz, J.; Hunt, D. F. (2004), *Int. J. Mass Spectrom.236*, 33–42.
98. Gunawardena, H. P.; He, M.; Chrisman, P. A.; Pitteri, S. J.; Hogan, J. M.; Hodges, B. D. M.; McLuckey, S. A. (2005), *J. Am. Chem. Soc. 127*, 12627–12639.
99. Liang, X. R.; Xia, Y.; McLuckey, S. A. (2006), *Anal. Chem. 78*, 3208–3212.
100. Coon, J. J. (2009), *Anal. Chem. 81*, 3208–3215.
101. Zubarev, R. A.; Haselmann, K. F.; Budnik, B.; Kjeldsen, F.; Jensen, F. (2002), *Eur. J. Mass Spectrom. 8*, 337–349.
102. Syrstad, E. A.; Turecek, F. (2005), *J. Am. Soc. Mass Spectrom. 16*, 208–224.
103. Martin, A. J. P.; Synge, R. L. M. (1941), *Biochem. J. 35*, 1358.
104. James, A. T.; Martin, A. J. P. (1952), *Biochem. J. 50*, 679.
105. James, A. T. (1952), *Biochem. J. 52*, 242.
106. James, A. T.; Martin, A. J. P.; Smith, G. H. (1952), *Biochem. J. 52*, 238.
107. Golay, M. J. E. (1958), in Coates, V. J.; Noebels, H. J.; Fagerson, I. S., eds., *Gas Chromatography*, Academic Press, New York, *1958*, pp. 1–13.
108. Gohlke, R. S. (1959), *Anal. Chem. 31*, 535.
109. Holmes, J. C.; Morrell, F. A. (1957), *Appl. Spectrosc. 11*, 86.
110. Niesson, W. M. A. (2001), *Current Practice of Gas Chromatography—Mass Spectrometry*, Marcel Dekker, New York.
111. Ryhage, R., *Anal. Chem.* (1964) *36*, 759.
112. Abian, J. (1999), *J. Mass Spectrom. 34*, 157.
113. Braithwaite, A. J.; Smith, F. J. (1996), *Chromatographic Methods*, 5th ed., Blackie, Glasgow.

114. De Hoffmann, E.; Stroobant, V. (2002), *Mass Spectrometry Principles and Applications*, 2nd ed., Wiley, Chichester, UK.
115. Hendrich, L. H. (1995), in Grob, R. L., ed., *Modern Practice of Gas Chromatography*, 3rd ed., Wiley, New York, pp. 265–321.
116. Niesson, W. M. A. (2006), *Liquid Chromatography—Mass Spectrometry*, 3rd ed., CRC Press, Boca Raton, FL.
117. Ardrey, B. (2003), *Liquid Chromatography—Mass Spectrometry: An Introduction*, Wiley, Chichester, UK.
118. McFadden, W. H.; Schwartz, H. L.; Evans, S. (1976), *J. Chromatogr. 122*, 389.
119. Scott, R. P. W.; Scott, C. G.; Munroe, M.; Hess, J., Jr., (1994), *J. Chromatogr. 99*, 395.
120. Tal'roze, V. L.; Karpov, G. V.; Gorodetskii, I. G.; Skurat, V. E. (1968), *Russ. J. Phys. Chem. 42*, 1658.
121. Baldwin, M. A.; McLafferty, F. W. (1973), *Org. Mass Spectrom. 7*, 1111.
122. Arpino, B.; Baldwin, M. A.; McLafferty, F. W. (1974), *Biomed. Mass Spectrom. 1*, 80.
123. Melera, A. (1980), *Adv. Mass Spectrom. 8B*, 1597.
124. Niesson, W. M. A. (1986), *Chromatographia 21*, 277.
125. Niesson, W. M. A. (1986), *Chromatographia 21*, 342.
126. Willoughby, R. C.; Browner, R. F. (1984), *Anal. Chem. 56*, 2626.
127. Cappiello, A. (1996), *Mass Spectrom. Rev. 15*, 283.
128. Caprioli, R. M.; Fan, T. (1986) *Anal. Chem*, *58*, 2949.
129. De Wit, J. S. M.; Deterding, L. J.; Moseley, M. A.; Tomer, K. B.; Jorgenson, J. W.; Caprioli, R. M. (1988), *Rapid Commun. Mass Spectrom. 2*, 100.
130. Ito, Y.; Takeuchi, T.; Ishii, D.; Goto, M. (1985), *J. Chromatogr. 346*, 161.
131. Caprioli, R. M.; Suter, M. J.-F. (1992), *Int. J. Mass Spectrom. Ion Process. 118/119*, 449.
132. Moseley, M. A.; Deterding, L. J.; De Wit, J. S. M.; Tomer, K. B.; Kennedy, R. T.; Bragg, N.; Jorgenson, *J. W.* (1989), *Anal. Chem. 61*, 1577.
133. Clegg, G. A.; Dole, M. (1971), *Biopolymers 10*, 821.
134. Dole, M.; Mack, L. L.; Hines, R. L.; Mobley, R. C.; Ferguson, L. D.; Alice, M. B. (1968), *J. Chem. Phys. 49*, 2240.
135. Mack, L. L.; Kralik, P.; Rheude, A.; Dole, M. (1970), *J. Chem. Phys. 52*, 4977.
136. Yamashita, M.; Fenn, J. B. (1984), *J. Phys. Chem. 88*, 4451.
137. Whitehouse, C. M.; Dreyer, R. N.; Yamashita, M.; Fenn, J. B. (1985), *Anal. Chem. 57*, 675.
138. Horning, E. C.; Horning, M. G.; Carroll, D. I.; Dzidic, I.; Stillwell, R. N. (1973), *Anal. Chem. 45*, 936.
139. Cody, R. B. (2002), in Pramanik, B. N., Ganguly, A. K., Gross, M. L.eds., *Applied Electrospray Mass Spectrometry*, Marcel Dekker, New York, pp. 1–105.
140. Emmett, M. R.; Caprioli, R. M. (1994), *J. Am. Soc. Mass Spectrom. 5*, 605.
141. Wilm, M.; Mann, M. (1996), *Anal. Chem. 68*, 1.
142. Gallagher, R. T.; Balogh, M. P.; Davey, P.; Jackson, M. R.; Sinclair, I.; Southern, L. J. (2003), *Anal. Chem. 75*, 973.
143. Jorgenson, J. W.; Lukacs, K. D. (1981), *Anal. Chem. 53*, 1298.
144. Jorgenson, J. W.; Lukacs, K. D. (1983), *Science 222*, 266.

145. Klampfl, C. W. (2006), *Electrophoresis 27*, 3.
146. Baker, D. R. (1995), *Capillary Electrophoresis*, Wiley, Chichester, UK.
147. Camilleri, P. (1993), *Capillary Electrophoresis Theory and Practice*, CRC Press, Boca Raton, FL.
148. Schmitt-Koplin, P. (2008), *Capillary Electrophoresis Methods and Protocol*, Humana Press, Totowai, NJ.
149. Shintani, H.; Polonský, J. (1997), *Handbook of Capillary Electrophoresis Applications*, Chapman & Hall, London.
150. Weinberger, R. (1993), *Practical Capillary Electrophoresis*, Academic Press, San Diego, CA.
151. Olivares, J. A.; Nguyen, N. T.; Yonker, C. R.; Smith, R. D. (1987), *Anal. Chem. 59*, 1230.
152. Maxwell, E. J.; Chen, D. D. Y. (2008), *Anal. Chim. Acta 627*, 25.
153. Schmitt-Koplin, P.; Frommberger, M. (2003), *Electrophoresis 24*, 3837.
154. Fanali, S.; D'Orazio, G.; Foret, F.; Kleparnik, K.; Aturki, Z. (2006), *Electrophoresis 27*, 4666.
155. Smith, R. D.; Barinaga, C. J.; Udseth, H. R. (1988). *Anal. Chem. 60*, 1948.
156. Álvarez-Llamas, G.; del Rosario Fernández de laCampa, M.; Sanz-Medel, A. (2005), *Trends Anal. Chem. 24*, 28.
157. Kannamkumarath, S. S.; Wrobel, K.; Wrobel, K.; B'Hymer, C.; Caruso, J. A. (2002), *J. Chromatogr. A 975*, 245.
158. Michalke, B. (2005), *Electrophoresis 26*, 1584.
159. Tanaka, Y.; Otsuka, K.; Terabe, S. (2003), *J. Pharm. Biomed. Anal. 30*, 1889.
160. Mol, R.; de Jong, G. J.; Somsen, *G. W.* (2005), *Electrophoresis 26*, 146.
161. Schmitt-Koplin, P.; Englmann, M. (2005), *Electrophoresis 226*, 1209.
162. Eiceman, G. A.; Karpas, Z. (2005), *Ion Mobility Spectrometry*, 2nd ed., CRC Press, Boca Raton, FL.
163. Kanu, A. B.; Dwivedi, P.; Tam, M.; Matz, L.; Hill, H. H., Jr., (2008), *J. Mass Spectrom. 43*, 1.
164. Collins, D. C.; Lee, M. L. (2002), *Anal. Bioanal. Chem. 372*, 66.
165. Cohen, M. J.; Karasek, F. W. (1970), *J. Chromatogr. Sci. 8*, 330.
166. Dwivedi, P.; Wu, C.; Matz, L. M.; Clowers, B. H.; Siems, W. F.; Hill, H. H., Jr., (2006), *Anal. Chem.*, *78*, 8200.
167. Guevremont, R.; Siu, K. W. M.; Wang, J.; Ding, L. (1997), *Anal. Chem. 69*, 3959.
168. Valentine, S. J.; Counterman, A. E.; Hoaglund, C. S.; Reilly, J. P.; Clemmer, D. E. (1998), *J. Am. Soc. Mass Spectrom. 9*, 1213.
169. Hoaglund, C. S.; Valentine, S. J.; Sporleder, C. R.; Reilly, J. P.; Clemmer, D. E. (1998), *Anal. Chem. 70*, 2236.
170. Ruotolo, B. T.; Gillig, K. J.; Stone, E. G.; Russell, D. H.; Fuhrer, K.; Gonin, M.; Schultz, J. A. (2002), *Int. J. Mass Spectrom. 219*, 253.
171. Steiner, W. E.; Clowers, B. H.; Fuhrer, K.; Gonin, M.; Matz, L. M.; Siems, W. F.; Schultz, A. J.; Hill, H. H., Jr., (2001), *Rapid Commun. Mass Spectrom. 15*, 2221.
172. Liu, Y.; Clemmer, D. E. (1997), *Anal. Chem. 69*, 2504.
173. Clowers, B. H.; Hill, H. H., Jr., (2005), *Anal. Chem. 77*, 5877.

174. Creaser, C. S.; Benyezzar, M.; Griffiths, J. R.; Stygall, J. W. (2000), *Anal. Chem. 72*, 2724.
175. Tang, X.; Bruce, J. E.; Hill, *H. H., Jr.* (2007), *Rapid Commun. Mass Spectrom. 21*, 1115.
176. Ouyang, Z.; Cooks, R. G. (2009), *Annu. Rev. Anal. Chem. 2*, 187–214.
177. Gao, L.; Song, Q. Y.; Patterson, G. E.; Cooks, R. G.; Ouyang, Z. (2006), *Anal. Chem. 78*, 5994–6002.
178. Gao, L.; Sugiarto, A.; Harper, J. D.; Cooks, R. G.; Ouyang, Z. (2008), *Anal. Chem. 80*, 7198–7205.
179. Gao, L.; Cooks, R. G.; Ouyang, Z. (2008), *Anal. Chem. 80*, 4026–4032.
180. Takats, Z.; Wiseman, J. M.; Gologan, B.; Cooks, R. G. (2004), *Science 306*, 471–473.
181. Cody, R. B.; Laramee, J. A.; Durst, H. D. (2005), *Anal. Chem. 77*, 2297–2302.
182. Venter, A.; Nefliu, M.; Cooks, R. G. (2008), *Trends Anal. Chem. 27*, 284–290.
183. Harper, J. D.; Charipar, N. A.; Mulligan, C. C.; Zhang, X. R.; Cooks, R. G.; Ouyang, Z. (2008), *Anal. Chem. 80*, 9097–9104.
184. Na, N.; Zhao, M. X.; Zhang, S. C.; Yang, C. D.; Zhang, X. R. (2007), *J. Am. Soc. Mass Spectrom. 18*, 1859–1862.
185. Takats, Z.; Cotte-Rodriguez, I.; Talaty, N.; Chen, H. W.; Cooks, R. G. (2005), *Chem. Commun.*, *15*, 1950–1952.
186. Huang, G.; Chen, H.; Zhang, X.; Cooks, R. G.; Ouyang, Z. (2007), *Anal. Chem. 79*, 8327–8332.
187. Chen, H. W.; Pan, Z. Z.; Talaty, N.; Raftery, D.; Cooks, R. G. (2006), *Rapid Commun. Mass Spectrom. 20*, 1577–1584.
188. Chen, H. W.; Talaty, N. N.; Takats, Z.; Cooks, R. G. (2005), *Anal. Chem. 77*, 6915–6927.
189. Garcia-Reyes, J. F.; Mazzoti, F.; Harper, J. D.; Charipar, N. A.; Oradu, S.; Ouyang, Z.; Sindona, G.; Cooks, R. G. (2009), *Rapid Commun. Mass Spectrom. 23*, 3057–3062.
190. Wiseman, J. M.; Puolitaival, S. M.; Takats, Z.; Cooks, R. G.; Caprioli, R. M. (2005), *Angew. Chem. Int. Ed. 44*, 7094–7097.
191. Wiseman, J. M.; Ifa, D. R.; Song, Q. Y.; Cooks, R. G. (2006), *Angew. Chem. Int. Ed. 45*, 7188–7192.
192. Wiseman, J. M.; Ifa, D. R.; Zhu, Y. X.; Kissinger, C. B.; Manicke, N. E.; Kissinger, P. T.; Cooks, R. G. (2008), *Proc. Natl. Acad. Sci. USA 105*, 18120–18125.
193. Wang, H.; Liu, J.; Cooks, R. G.; Ouyang, Z. (2008), *Angew. Chem. Int. Ed. 49*, 877–880.
194. Plass, W. R.; Li, H. Y.; Cooks, R. G. (2003), *Int. J. Mass Spectrom.*, *228*, 237–267.
195. Maxwell, E. J.; Chen, D. D. Y. (2008), *Anal. Chim. Acta 627*, 25.
196. Karpas, Z.; Stimac, R. M.; Rappoport, Z. (1988), *Int. J. Mass Spectrom. Ion Process. 83*, 163–175.
197. Chen, H.; Venter, A.; Cooks, R. G. (2006), *Chem. Commun.* 2042–2044.
198. Chen, H. W.; Venter, A.; Cooks, R. G. (2006), *Chem. Commun.* 2042–2044.
199. Shiea, J.; Huang, M.-Z.; HSu, H.-J.; Lee, C.-Y.; Yuan, C.-H.; Beech, I.; Sunner, J. (2005), *Rapid Commun. Mass Spectrom. 19*, 3701–3704.
200. Andrade, F. J.; Wetzel, W. C.; Webb, M. R.; Gamez, G.; Ray, S. J.; Hieftje, G. M. (2008), *Anal. Chem. 80*, 2654–2663.